Review

# Integrated laser technologies for artificial intelligence applications [Invited]

CHANGHAO HAN, MINGXIAO LI, D JOEL GUO, D AND JOHN E. BOWERS D

Department of Electrical and Computer Engineering, University of California, Santa Barbara, California 93106, USA

\*bowers@ece.ucsb.edu

**Abstract:** The development of emerging artificial intelligence (AI) technologies has led to an increase in data volumes, placing higher requirements for information photonic systems. Integrated lasers are core functional components in photonics to provide optical signals. Here, we review integrated laser technologies for AI applications, from device to system level. In the beginning, we summarized the transmitter technologies, trends, and requirements, which are the primary driving forces for lasers. Then, we discussed integrated III-V lasers based on different photonic platforms in detail. For the system level, we summarized the recent progress of representative applications for AI based on integrated laser technologies.

© 2025 Optica Publishing Group under the terms of the Optica Open Access Publishing Agreement

#### 1. Introduction

In recent years, with the rapid development and application of the emerging information and communication technologies (ICT) represented by artificial intelligence (AI), cloud computing, big data, and internet of things (IOT), the total amount of global data has continued to grow significantly, which has put forward higher requirements on the speed and capacity of data communication links [1,2]. According to a global data research report released by global information agency IDC, the global data circle has grown to 175 ZB by 2025 [3]. With the evolution of the modern information society, as the basic supporting facilities in the AI era for digital economy, the current traditional communication systems are facing the pressure and challenges of upgrading speed and capacity [4]. For example, to train AI models such as ChatGPT, increasingly GPUs need to be deployed, and the total bandwidth of the next-generation interconnection module needs to reach the P-bit level or above [5–7]. Under this background, optical communication technology can build optical networks for high-speed data transmission with its advantages of high bandwidth, large capacity, low power consumption, low loss and low crosstalk, which have occupied an irreplaceable position in ICT networks [8]. However, the devices in traditional optical communication systems are composed of discrete devices with large size, while the system complexity increases rapidly with the continuous expansion of network capacity. Therefore, in the context of the AI era, it has become an industry consensus to integrate various photonics devices on photonic integrated circuits (PICs) through integration technology to realize high-density, low-cost, and low-energy chip-scale optoelectronic information systems [9-11].

In photonics systems, lasers are the core active functional components to provide light signals [12], and the rapid development and widespread application of optical communications rely on semiconductor lasers [13,14]. III-V materials such as indium phosphide (InP), gallium arsenide (GaAs) and gallium nitride (GaN) are the preferred materials due to their high gain and high efficiency resulting from their direct bandgap [15,16]. Integrated III-V laser technologies represented by distributed feedback (DFB) and distributed Bragg reflector (DBR) laser chips can replace traditional bench-top lasers to provide optical carriers in various photonic systems, thereby greatly reducing system size and energy consumption [17,18], and native III-V substrate

PICs [19–21] have already achieved deployment in ICT industrial applications [22–24]. However, limited by the relatively small wafers (e.g. 150 mm diameter for InP, 200 mm diameter for GaAs) [25], the manufacturing cost of III-V material systems is still relatively high compared with silicon (Si) (typically 300 mm diameter) [26], while the high loss as well as the small index contrast for the III-V-based waveguides constrains the design of III-V-based large-scale optoelectronic systems [27].

In contrast, as a low-cost wafer-scale optoelectronic integration platform, Si photonics technology utilizes Si-based materials as substrates and functional materials, which has attracted continuous attention from academia and industry because of its advantages such as low power consumption, high density, low cost, high electrical scalability and complementary metal oxide semiconductor (CMOS) compatibility [28-30]. While the Si platform is very suitable for passive devices [31–33], a variety of functional active devices based on Si photonics have been successfully demonstrated with development over the years, including modulators [34–38] and detectors [39–43], and have shown a series of advantages in both performance and integration. However, the fabrication of Si-based lasers has still been elusive over decades due to the indirect bandgap of Si [44-46]. Although Si PICs have made impressive progress in large-scale complex photonics systems in recent years, the light source in most works is not integrated which limits the system size and complexity [47,48]. For laser integration in Si photonics, there are currently two mainstream types: hybrid integration and heterogeneous integration [49–51]. Hybrid integration refers to an assembling approach after the chip fabrication process, where one separate PIC (e.g. III-V laser chip) is integrated with another functional Si PIC through optical alignment and packaging. At the practical application level, the hybrid integration between separately fabricated III-V laser chips (single or array) and Si PICs on one single packaging substrate board is an effective solution to achieve the miniaturization of the entire optoelectronic system and has become the common solution for today's Si photonic modules (including light sources) [50]. However, although this approach is engineering-feasible and improves size and power consumption, it is not truly integration on one single chip, while still facing fabrication and scalability challenges (such as array precision alignment). In essence, hybrid integration moves the problems of nanophotonic manufacturing to the subsequent packaging stage, while the preparation of integrated laser chips based on III-V material substrates still has relatively high costs. On the other aspect, heterogeneous integration refers to the transfer of non-Si material onto the Si substrate through wafer bonding technology in the fabrication process, thereby realizing the target functional systems on one single chip [51]. With the development of nanophotonic manufacturing technology, research on heterogeneously integrated lasers has increased and achieved a series of breakthroughs these years. In fact, the heterogeneously III-V integrated lasers can be conducted not only on pure Si platforms [52], but also on the silicon nitride (SiN) [53] and thin film lithium niobate (TFLN) [54] platforms as well to realize photonic systems with different functional orientations. In contrast to pure III-V-based photonics integration, although integrating multiple materials on one same substrate will inevitably increase the complexity of the process, heterogeneous integration can be performed on silicon-on-insulator (SOI) with large wafer area to provide lower cost and higher reliability [55,56]. To a certain extent, adopting native III-V substrate PICs as a primary scaling direction for AI systems presents challenges, especially when considering the cost and scalability of the platform. Instead, the industry trend is to heterogeneously integrate III-V gain with scalable platforms, such as Si for CMOS-compatible process, SiN for ultra-low-loss routing, and TFLN for high-linearity, high-bandwidth modulation. This division of roles combines wafer-scale process control, mature process design kit (PDK), low propagation loss, high thermal stability, and supply-chain robustness with the unique ability of III-V materials to provide efficient light sources and on-chip gain. Accordingly, this work mainly focuses on integrated lasers on different scalable platforms including Si/SiN/TFLN, to meet the system-level requirements for AI applications. In AI systems, co-integrating on-chip optical

amplification with lasers on one single PIC preserves link budgets for optical interconnections and computing. Meanwhile, although heteroepitaxial growth of III-V lasers on Si directly is not yet commercially viable, it is a promising and rapidly developing approach for laser integration in AI applications.

In this paper, we focus on integrated laser technologies for emerging AI applications. We start with transmitter technologies, trends, and requirements, which is the key scenario for AI and the main driving force for integrated lasers. Next, we review the progress of integrated III-V lasers based on different photonic platforms including Si, SiN and TFLN. Hybrid integration and heterogeneous integration are both analyzed comprehensively. Furthermore, the representative applications for AI including optical interconnections, optical neural networks and on-chip light detection and ranging (LiDAR) systems based on integrated laser technologies are discussed and summarized in detail.

#### 2. Transmitter technologies, trends, and requirements

Under the background of data growth brought about by AI, for integrated optoelectronics including lasers, transmitter technology remains the entry point and driving force to large-scale commercialization. In transmitter architecture, lasers and electro-optical (EO) modulators are key components for data transmission, where the laser provides the optical signal and the modulator converts the high-speed radio frequency (RF) signals into the optical domain [57]. The EO modulator has a significant impact on the practical transmission performance of the transmitter [36]. Here, different types of integrated modulators are analyzed to illustrate the technical progress and trends of transmitters, as well as the requirements of wavelength division multiplexing (WDM) systems for integrated lasers.

#### 2.1. Integrated pure Si modulators

Pure Si modulators are based on standard Si photonic platforms and achieve modulation function by doped Si, relying on the plasma dispersion effect [35]. Due to the advantages of large-scale production, high stability, low cost and high electrical scalability, pure Si modulators have been the research focus of transmitter technologies [34]. Si modulators can be divided into Si Mach-Zehnder modulators (MZMs) and Si microring modulators (MRMs), according to different optical architectures.

Si MZMs can be constructed based on the Mach-Zehnder interferometer (MZI) structure, which converts the phase change of light into intensity change through the principle of optical interference. Si MZMs have advantages of good thermal stability, large extinction ratio (ER), large operating wavelength range, small chirp, and low sensitivity to process errors. The first integrated Si MZM operating at 1 GHz was demonstrated by Intel in 2004 [58], based on metal-oxide-semiconductor (MOS) structure, and significant breakthroughs have been made in transmission speed over the past two decades. Several methods are proposed to enhance the modulator performance including bandwidth and modulation efficiency, such as slow wave electrodes [59] and interleaved PN junction structures [60]. Representatively, in 2018, M. Li et al. adopted the improved substrate removal fabrication process to reduce the RF transmission loss and realize better matching of EO group index and impedance [61], achieving 90 Gbps on-off keying (OOK) and 112 Gbps 4-level pulse amplitude modulation (PAM-4) transmission. At the photonic-electric integration level, in 2020, H. Zhang et al. packaged the 4-channel high-bandwidth Si modulator chip with the electrical driver chip together [62], and 200 Gbps PAM-4 transmission is demonstrated per lane in 1 km standard single-mode fiber (SSMF). In 2023, K. Li et al. demonstrated a photonic-electric integrated Si transmitter [63], where a switching current is applied to the passive equalization guided Si MZMs. A series of transmitters are fabricated on the same wafer, including the 1.27 mm U-shaped transmitter, 2.47 mm U-shaped transmitter and segmented transmitter with two different phase-shifter lengths for PAM-4, shown

in Fig. 1(a). High-speed transmission of 112 Gbps OOK and 224 Gbps PAM-4 transmissions are achieved with energy consumption below 1 pJ/bit. In fact, segmenting the phase shifter to construct a segmented Si modulator is a representative way to increase the transmission performance [64]. In 2023, A. Mohammadi et al. used a three-segment MZI structure with a length of 2 mm each to design a high-bandwidth Si segmented modulator in Fig. 1(b) [65]. The EO bandwidth is increased to 67 GHz and ultrahigh-speed signal transmission of 360 Gbps is realized based on 8-level amplitude shift keying (8-ASK) signal format. However, a sufficiently long modulation arm is required for MZI in above designs, which results in a large footprint of the modulator.

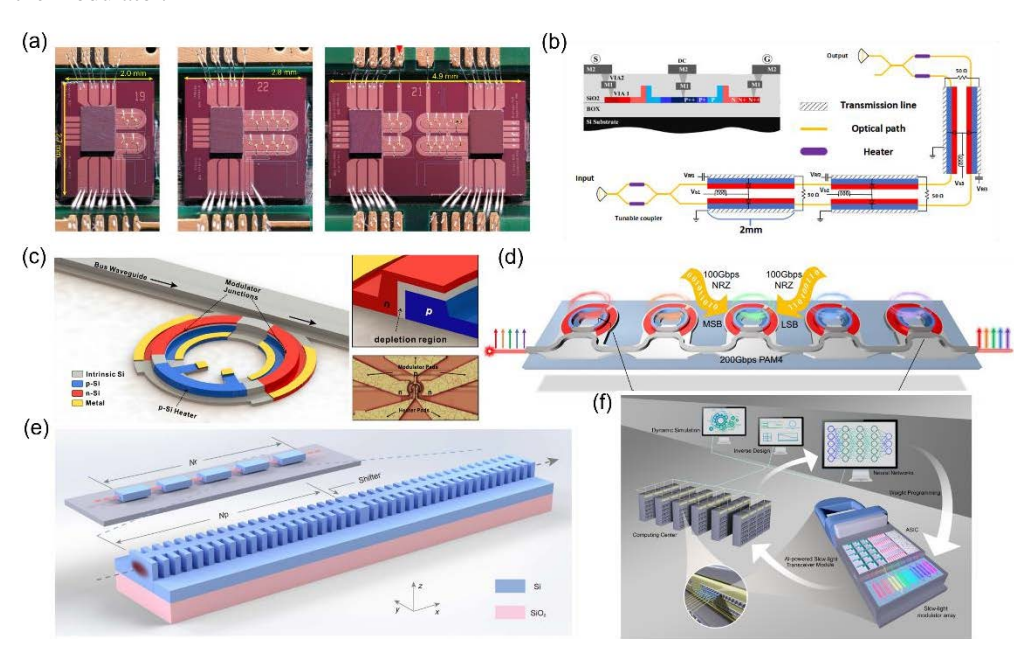


**Fig. 1.** Integrated pure Si modulators. (a) Optical micrograph of the co-packaged Si MZM transmitter. The 1.27 mm U-shaped transmitter, 2.47 mm U-shaped transmitter, segmented transmitter with two different phase-shifter lengths for PAM-4 are illustrated. Reprinted from Ref. [63]. (b) Schematic of the segmented Si MZM. The EO bandwidth is increased to 67 GHz and 360 Gbps signal transmission is realized. Reprinted from Ref. [65]. (c) Schematic of the tunable Si MRM. Two segments of PN junctions and one segment of heater are shown. The PN junctions are optimized to increase the overlap with the optical mode. Reprinted from Ref. [69]. (d) Schematic of the 5-channel WDM Si two-segment MRM array. 200 Gbps PAM-4 transmission per lane is achieved with a total data capacity of 1 Tbps. Reprinted from Ref. [72]. (e) Schematic of the high-speed Si slow-light modulator with 110 GHz bandwidth. The slow-light waveguide consists of Bragg gratings separated by phase shifter regions on SOI wafer. Reprinted from Ref. [74]. (f) Conceptual drawing of the AI-accelerated Si photonic slow-light technology. The AI-accelerated slow-light transmitter module provides an ultrahigh-speed solution for optical interconnections in computing centers. Reprinted from Ref. [75].

In contrast, Si MRMs have smaller device size and lower power consumption, which is conducive to the design of integrated systems [66]. The integrated Si MRM was proposed in 2005 [67], which is based on a resonant cavity structure and achieves modulation through coupling between a doped microring and a straight waveguide [68]. In recent years, Si MRMs provide a competitive compact-size and low-power solution for dense optoelectronic integration, while the transmission rate maintains a favorable level. In 2019, Intel demonstrated a tunable 50 GHz

Si MRM with a transmission rate of 128 Gbps PAM-4 [69]. The PN junction is optimized to form a depletion region in both vertical and horizontal directions to increase the modulation efficiency to  $0.52~\rm V\cdot cm$ , as shown in Fig. 1(c). In 2022, D. Chan et al. reported a Si MRM with a bandwidth of 67 GHz, with a compact size of  $24~\mu m \times 70~\mu m$  [70]. By utilizing the optical peak effect and negative chirp, 200 Gbps PAM-4 high-speed signal transmission is achieved in 2 km SSMF. Furthermore, in 2023, they achieved 330 Gbps ultrahigh-speed 8-level pulse amplitude modulation (PAM-8) signal transmission based on a high-bandwidth Si MRM, while the driving voltage was only 1.8 Vpp, thus ensuring a low energy consumption of 3.1 fj/bit [71]. In 2024, Y. Yuan et al. demonstrated a WDM Si two-segment MRM array with an optimized Z-shape doping [72], shown in Fig. 1(d), while 200 Gbps PAM-4 per lane is achieved with a total data capacity of 1 Tbps and a low energy consumption of 6.3 fJ/bit. However, due to the limitation of photon lifetime of microring resonator, the optical bandwidth of Si MRMs is very small, typically less than 1 nm, which makes the Si MRMs temperature sensitive. In practical systems, a temperature control module is usually required, thus increasing the energy consumption budget of the system.

Although pure Si modulators have a high degree of CMOS compatibility, which brings the cost advantages in production process, the limited plasma dispersion effect usually hinders their performance at high frequencies [73]. In terms of new optical architectures for high-speed scenarios, in 2023, C. Han et al. designed a high-speed Si slow-light modulator with an EO bandwidth of 110 GHz based on the standard Si photonic process with an ultra-compact size of only 124 µm [74]. The slow-light waveguide structure is demonstrated in Fig. 1(e). The compact slow-light modulator can achieve high-speed signal transmission beyond 110 Gbps OOK without digital signal processing (DSP) at 1550 nm, and maintains high stability of multi-wavelength performance within an optical passband of 8 nm. Furthermore, based on a multi-channel Si slow-light modulator chip, PAM-4 optical transmission of 400 Gbps per wavelength is realized with the utilization of AI network equalizers [75], leading to a total data capacity of 3.2 Tbps with an on-chip data-rate density of 1.6 Tb/s/mm². This ultrahigh-speed result demonstrates the great potential of Si photonics in the future 3.2 T era. Simultaneously, the AI-accelerated Si photonic technology, shown in Fig. 1(f), is an example of AI applications in photonics, and illustrates the potential of cross-disciplinary research in AI and photonics.

#### 2.2. Integrated heterogeneous modulators

The above research is on pure Si modulators based on single material systems. Although pure Si modulators have industrial advantages and electrical scalability brought by high CMOS compatibility, their performance still has certain limitations, especially for high-speed applications. Also, realizing effective on-chip lasers based on pure Si material systems remains a long-standing problem in Si photonics due to the indirect bandgap property of Si. With the development and application of Si modulators, it is essential to find efficient on-chip laser solutions on Si platforms. Therefore, developing new methods to improve modulator performance on heterogeneous platforms with multiple materials is an effective route to significantly enhance overall device performance. More importantly, the heterogeneous integration platform provides a foundation for the subsequent on-chip light sources, thus constructing a fully integrated transmitter as well as different photonic systems with other functions.

Achieving high-integration and high-speed transmission while ensuring low cost and scalability is promising with heterogeneous platforms. In recent years, by introducing heterogeneous materials with favorable EO performance on low-cost Si-based substrate, such as TFLN [76,77], organic polymers [78,79], germanium (Ge) [80,81] and III-V materials [50,82], research on constructing heterogeneous integrated modulators has continued to increase, and a series of high-performance breakthroughs have been achieved. The realizations of integrated heterogeneous modulators with impressive high-speed performance also encourage researchers to develop high-efficiency integrated lasers on heterogeneous platforms.

As a high-quality EO material with excellent Pockels effect, lithium niobate (LN) has been widely used in the optoelectronics field over decades and is the preferred material for conventional EO modulators [83]. In recent years, the process of preparing TFLN on Si substrates has become increasingly mature [84] and the high index contrast achievable with TFLN results in higher confinement, smaller modes and lower drive voltages and lower loss. Si-based TFLN modulators have achieved a high degree of integration compared to traditional LN modulators and demonstrated impressive performance especially high-speed transmissions [85]. Representatively, in 2018, C. Wang et al. demonstrated a Si-based TFLN modulator with an ultra-high EO bandwidth of 100 GHz with a half-wave voltage of 4.4 V for a modulation arm of 5 mm, achieving 140 Gbps 4-level amplitude shift keying (4-ASK) and 210 Gbps 8-ASK transmissions, shown in Fig. 2(a) [86]. In 2019, M. He et al. reported a Si-based TFLN modulator with an EO bandwidth exceeding 70 GHz, a modulation efficiency of 2.2 V·cm and an insertion loss of 2.5 dB, realizing 100 Gbps OOK and 112 Gbps PAM-4 transmissions [87]. Due to the linear EO properties of TFLN, the modulator has a high linearity, with a spurious-free dynamic range (SFDR) of 99.6 dB·Hz<sup>2/3</sup> in the third-order intermodulation distortion (IMD3) at 1 GHz. However, compared to pure Si modulators, the modulation efficiency is still not sufficient, and a long modulation arm is required for decreasing the half-wave voltage (7.4 V for 3 mm and 5.1 V for 5 mm) [87]. Despite this, in recent years, the performance of Si-based TFLN modulators has improved greatly, especially in high-speed applications. Currently, TFLN modulators with EO bandwidths around 110 GHz [88–93] and single-lane transmission rates exceeding 400 Gbps have been developed [94–98], while the high modulation efficiency around and below 1.0 V·cm has also been achieved with the half-wave voltage of around 2 V [92,93]. For system-level transmissions beyond 400 Gbps, the integrated uncooled DFB lasers can be adopted as light sources to increase integration level, while maintaining sub 1-V driving voltage from a 3 nm CMOS SerDes [96,98]. This demonstrates the potential of the TFLN platform for next-generation interconnections, which can achieve ultra-high transmission rates beyond 400 Gbps under low energy consumption conditions with integrated light sources and low driving voltages. On the other hand, from the perspective of heterogeneous integration, as a preferred modulation material, TFLN can be integrated not only on Si platforms, but also on SiN platforms with low loss [99,100]. In 2023, Z. Ruan et al. demonstrated a LN/SiN heterogeneous modulator with a modulation bandwidth of 37 GHz, a half-wave voltage of 4.3 V and a low insertion loss of 1 dB, achieving 128 Gbps PAM-4 transmission [101]. The device structure is shown in Fig. 2(b). The combination of TFLN and SiN compensates for the difficulty of fabricating modulators on SiN platforms while retaining the advantage of ultra-low loss.

Organic polymer materials with high EO coefficient can be used as functional materials to improve the performance of Si-based modulators [102]. By combining polymers with Si-based platforms, the bandwidth, modulation efficiency and energy consumption of the modulator can be significantly improved. In 2014, L. Alloatti et al. demonstrated a Si-based organic polymer modulator in Fig. 2(c), with an EO bandwidth of 100 GHz and a modulation efficiency of 1.1 V·cm, achieving 120 Gbps PAM-4 and 400 Gbps 16-level quadrature amplitude modulation (16-QAM) signal transmission [78]. Despite this, the unstable organic polymer materials will usually face the issue of poor temperature stability. To solve this problem, in 2020, G. Liu adopted a type of polymer with both high EO coefficient and high transition temperature to improve the temperature stability of Si-based organic polymer modulators, shown in Fig. 2(d) [79]. The modulator can operate normally for 200 Gbps PAM-4 transmission at 110°C and can continue to work for 100 hours at 90°C. Furthermore, in 2022, a high-temperature-resistant Si-based organic polymer modulator is realized with a length of 0.75 mm and a modulation efficiency higher than 0.5 V·mm, which can work for more than 5000 hours in an environment of 85°C [103]. It can be seen that if Si-based polymer modulators are to be further applied on a large scale, the temperature stability of polymers needs to be improved to work in the high

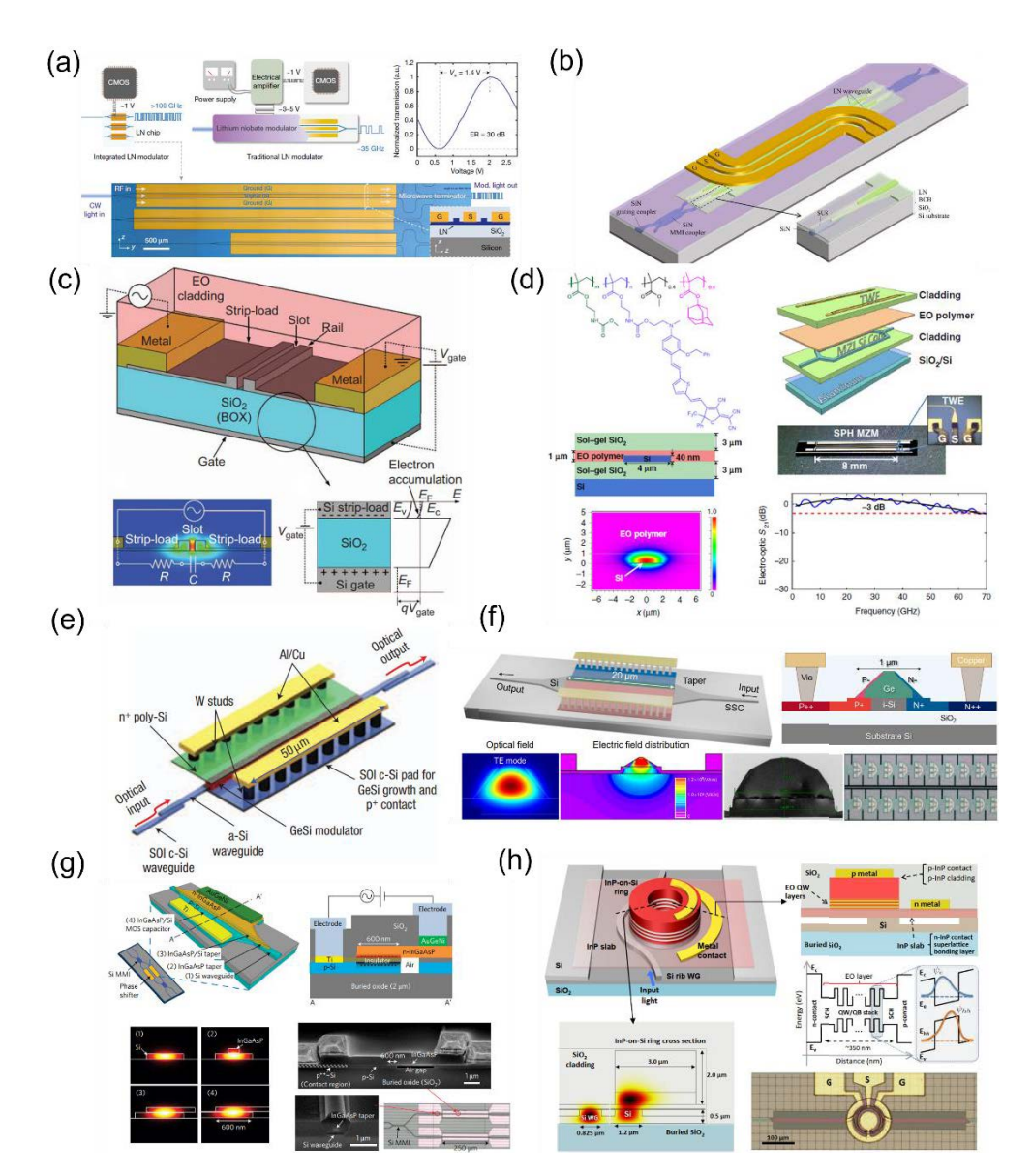


Fig. 2. Integrated heterogeneous modulators. (a) Si-based TFLN modulators compatible with CMOS drive voltages. The integrated TFLN modulators can get performance enhancement compared to traditional LN modulators. Reprinted from Ref. [86]. (b) Schematic of the LN/SiN heterogeneous modulator. The LN waveguide is integrated on SiN platform to achieve modulation functions. Reprinted from Ref. [101]. (c) Schematic of the high-bandwidth Si-based polymer modulator. The EO polymer cladding covers the slot waveguide. Reprinted from Ref. [78]. (d) High temperature resistant Si-based polymer modulator. The molecular structure of the EO polymer and the device structure are shown. Reprinted from Ref. [79]. (e) Schematic of the waveguide-integrated GeSi modulator. The device length is only  $50\,\mu m.$  Reprinted from Ref. [80]. (f) Schematic of the high-speed GeSi modulator. The device structure and characterization diagram are shown. Reprinted from Ref. [81]. (g) Device structure of the III-V/Si MOS modulator. The introduction of III-V compound can increase modulation efficiency effectively due to the large electron-induced refractive index change. Reprinted from Ref. [115]. (h) The integrated cryogenic MRM on the heterogeneous III-V/Si platform. The modulator can achieve Gbps-level data rates under mV-level driving voltages at a temperature of 4 K. Reprinted from Ref. [118].

temperature environment of data centers, while maintaining the uniformity of overall device performance. Similar to the LN situation, the polymer can also be integrated on SiN, and the compact MRM with a bandwidth of 32 GHz and a data rate of 40 Gbps was achieved based on SiN platforms [104]. Although SiN is not good at EO modulation, the heterogeneous integration of EO functional materials provides the feasibility of high-speed modulation.

By introducing Ge material on Si substrates, a Si-based Ge (GeSi) modulator can be fabricated based on electro-absorption (EA) effect, which has the advantages of fast response speed, small size, and low power consumption. The first compact GeSi modulator in Fig. 2(e) was realized by IMEC in 2008, with a bandwidth of 1.2 GHz, a device length of 50  $\mu m$  and a low energy consumption of 50 fJ/bit, which is based on Franz-Keldysh (FK) effect [80]. In recent years, GeSi modulators have demonstrated favorable high-speed performance. In 2022, Chan et al. reported a high-bandwidth GeSi modulator with a size of only  $40\,\mu m \times 20\,\mu m$ , which has an EO bandwidth of 65 GHz and achieved 224 Gbps PAM-4 signal transmission in C-band [105]. In 2023, X. Hu et al. reported a GeSi modulator with an ultra-high EO bandwidth of 110 GHz, as shown in Fig. 2(f). The modulation arm size is only 20  $\mu m$  and 148 Gbps OOK and 280 Gbps PAM-4 transmission is achieved, with an energy consumption of only 12 fj/bit, demonstrating the great potential of GeSi modulators in the low-power ultrahigh-speed field.

In the optoelectronics fields, III-V materials such as InP and GaAs, are common functional materials that have been widely used in various active devices including lasers, amplifiers and modulators [50]. The modulation principle of III-V materials is based on Quantum-confined stark effect (QCSE). The light absorption can be changed by electric field, thus the III-V electroabsorption modulator (EAM) can be fabricated [82]. More importantly, for integrated III-V modulators, the luminescence advantages of III-V materials make modulators easy to integrate with on-chip lasers, while maintaining impressive high-speed performance [106]. Therefore, by integrating EAM and DFB, electro-absorption modulated laser (EML) can be constructed to provide a promising solution for optical interconnections. Due to the favorable EO performance of III-V materials, EMLs exhibit a series of advantages including compact footprint, high bandwidth, low power consumption and high integration level [107]. With the development over years, EML technology has become relatively mature and has entered commercialization, achieving a relatively high transmission rate [108,109]. In recent years, beyond 400 Gbps PAM-4 and PAM-8 transmissions are achieved based on an EML with sub 1 V driving voltage around 55°C [110–112]. Especially, in 2025, ultrahigh-speed transmission of 540 Gbps PAM-8 per lane in 30 km SSMF is achieved for the first time based on an EML with an EO bandwidth exceeding 110 GHz [113]. However, although integrated with on-chip DFB lasers, the above EML results are still based on InP substrates. Due to limited wafer area, III-V devices are less cost-effective than Si photonic, and the complex process constrains the electrical scalability for large-scale optoelectronic systems. Therefore, with the development of heterogeneous process, integrating III-V functional devices including modulators and lasers on Si-based substrates has become a research trend. To improve the insufficient modulation efficiency of Si modulators, some heterogeneously integrated III-V/Si MOS modulators were demonstrated, achieving effective enhancement in modulation efficiency for high-speed transmission to achieve compact footprint and low energy consumption. In 2017, J. Han et al. presented an InGaAsP /Si MOS MZM by direct wafer bonding, with an ultra-high modulation efficiency of 0.047 V·cm and optical attenuation of only 0.23 dB [114]. The introduction of III-V compound can increase modulation efficiency effectively due to the large electron-induced refractive index change compared to Si. In the same year, T. Hiraki et al. demonstrated an InGaAsP /Si MOS MZM with a 250-µm modulation length, a modulation efficiency of 0.09 V·cm, a bandwidth of 2.2 GHz and an optical loss of 1.0 dB, achieving 32 Gbps OOK transmission [115]. The device structure of the III-V/Si MOS modulator is shown in Fig. 2(g). For the modulation bandwidth improvement, in 2022, H. Tang et al. analyzed the impact of parasitic capacitance on the bandwidth of the III-V/Si MOS

modulator and demonstrated an InGaAsP/Si modulator with a low capacitance [116]. The device has a bandwidth of  $10\,\mathrm{GHz}$ , with a modulation efficiency of  $0.245\,\mathrm{V}\cdot\mathrm{cm}$ , realizing 40 Gbps PAM-4 transmission. In 2022, R. Koscica et al. presented a heterogeneous III-V/Si modulator in C-band, realizing 12 Gbps OOK transmission with 63 fJ/bit energy efficiency [117]. In the same year, P. Pintus et al. demonstrated an integrated cryogenic MRM on the heterogeneous III-V/Si platform for superconducting electronics and quantum systems, shown in Fig. 2(h) [118]. The modulator can achieve Gbps-level data rates under  $10\,\mathrm{mV}$  driving voltages at a temperature of 4 K, with an electric energy consumption of  $10.4\,\mathrm{aJ/bit}$  and an optical energy consumption of  $213\,\mathrm{fJ/bit}$ .

#### 2.3. Optical power budget for modulation

The previous discussions demonstrate the optical and electrical parameters of different modulator types at device level in the transmitter architecture. For the link perspective, the optical power and relative intensity noise (RIN) required from the laser will scale with the modulation symbol rate and format, which will directly influence the laser selections in transmitters [119,120]. Accordingly, the relationship of modulator parameters between laser optical power and RIN budget in IM/DD and coherent regimes will be briefly discussed here.

To keep the treatment consistent across links, the laser RIN is considered as a single-sideband spectrum and as an integrated value over the receiver's electrical bandwidth [120,121]. For IM/DD links, the integration window excludes the low-frequency 1/f region via alternating current (AC) coupling and extends to the receiver 3-dB bandwidth, therefore the RIN reflects the noise that affects link margin. The RIN within this window degrades signal-to-noise ratio (SNR) and therefore raises the required optical power, with higher symbol rates and multi-level formats increasing sensitivity [122,123]. For coherent links, system design is primarily influenced by optical signal-to-noise ratio (OSNR), yet an integrated RIN figure is still specified over the coherent receiver bandwidth to limit the residual amplitude noise under finite detector imbalance and signal-local oscillator (LO) beating. The balanced detection will improve LO-RIN sensitivity, while linewidth and phase noise become the dominant constraints [124,125].

The optical power requirement in the transmitter is set by the SNR needed to achieve the target bit error rate (BER) and thus scales with both data rate and modulation format [120,126]. In IM/DD architectures, increasing symbol rate broadens the receiver noise bandwidth and typically reduces available electrical swing from the driver at high frequency. To preserve link margin, the system must compensate by raising input power, reducing insertion loss in the modulator and couplers, and improving effective modulation depth and linearity [127,128]. These pressures are exacerbated for multi-level signaling, where PAM-4 and PAM-8 typically require additional SNR and optical modulation amplitude (OMA) improvements compared to OOK to overcome the smaller eye opening and linearity penalties [37]. Consequently, the laser parameters including RIN, ER, and power stability become more critical, and thermal control and DSP equalization are needed to avoid excessive optical power.

On the other hand, coherent links are governed primarily by OSNR compared to OMA [129]. For example, higher-order QAM can operate at lower per-channel optical power for a given transmission reach but imposes tighter constraints on laser linewidth, phase noise, I/Q bias stability, and inter-channel power flatness [130]. When multi-wavelength sources such as on-chip microcombs are employed, linewidth, RIN, and power uniformity directly translate into the impact for DSP complexity and energy consumption at the system level [131,132]. Therefore, as data rate increases and formats advance, IM/DD links tend to compensate in optical power unless insertion loss and effective modulation depth are improved, whereas coherent links shift the burden to OSNR, linewidth, phase noise, and channel-power equalization. These considerations inform the comprehensive selections and design strategies in lasers for AI applications in the following sections.

#### 2.4. Laser requirements in WDM systems

For data center markets, in addition to high-performance modulators, WDM is the economically viable path to Tbps-class optical I/O [128,133]. WDM systems, including coarse wavelength-division multiplexing (CWDM) and dense wavelength-division multiplexing (DWDM), are foundational to scaling optical I/O for AI systems [37,127,134]. WDM raises aggregate throughput per fiber and reduces fiber count without excessively increasing DSP cost, which is critical for port densities and rack-level bandwidth in modern AI hardware. Therefore, the transmitter module design is mostly based on WDM channel plans, which dictate requirements on parameters such as linewidth, RIN, power flatness and thermal stability for integrated lasers.

In CWDM, short-reach O-band links typically employ IM/DD with 4-8 wavelengths per fiber [135,136]. For the laser side, high conversion efficiency, low RIN and sufficient ER are required to achieve cost-effective pluggable and co-packaged transmitter modules. For instance, the quantum-dot mode-locked lasers (QD-MLLs) (The MLL refers to a laser that emits a comb of mode-locked lines, and multi-line emission can reduce the number of discrete sources in WDM systems) provide a competitive route for CWDM since they can supply multiple O-band lines with low RIN and favorable temperature tolerance, generating carriers for multi-lane IM/DD while simplifying thermal control and freeing power budget for DSP [127,137]. On the other hand, DWDM targets higher spectral efficiency and longer transmission distances, which can be combined with coherent modulation and 50-100 GHz channel spacing in C-band. Notably, on-chip microcombs provide tens to hundreds of evenly spaced carriers from a single optical source, enabling dense wavelength packing for transceivers [132]. The microcomb quality, including linewidth, RIN and power flatness will directly reduce DSP consumption and improve energy efficiency for the system level [128,131].

Therefore, both as multi-wavelength sources, QD-MLLs are more suitable for O-band CWDM while on-chip microcombs match well with C-band DWDM. The laser metrics (linewidth, RIN, line spacing, temperature stability) are related to the system-level indicators (channel count, transmission distance, spectral efficiency, and energy per bit). For AI-system level, the choices of lasers and WDM will directly influence the bandwidth together with energy efficiency, both for cloud training and terminal equipment. In computing centers, large-model training and fine-tuning rely on high-bandwidth operations, where CWDM IM/DD links push integration density for short-reach I/O, and DWDM coherent links extend reach within networks. For instance, selecting promising multi-wavelength sources such as QD-MLLs for CWDM IM/DD and microcombs for DWDM coherent transmissions, thus aligns the laser stack with AI workloads from front-end perception to system-scale interconnections, and provides a path for lower energy consumption and higher effective throughput.

# 3. Integrated lasers based on photonic platforms

For AI systems, the most important factors are bandwidth, energy per bit, long-term stability and scalability. The output power and EO conversion efficiency of integrated lasers determine the optical budget and dominate the energy per bit as channels expand. Linewidth and phase/frequency noise raise the OSNR required to reach the target BER and reduce DSP margin of coherent links, while RIN limits the IM/DD eye opening. As the number of channels increases, wavelength/thermal stability determines static tuning power and maintenance costs. Also, yield, aging, and reflectance tolerance will directly impact system cost and maintainability. Formulating specifications in this way clarifies how the laser performance improvements (e.g., narrower linewidth or higher output power) in Si, SiN, and TFLN platforms will deliver different system benefits.

#### 3.1. Integrated III-V lasers on Si

Si photonics technology has the advantages of low loss, low cost and compatibility with CMOS processing, electronics and packaging, which has been widely regarded as the promising solution for on-chip optical systems for large-scale deployment [30]. Considering the significant value of Si platforms, Si-based light source solutions have been the research focus of academic and industrial researchers in the photonic field [52]. From an engineering perspective, hybrid integration of III-V laser chips and Si PICs through packaging is common in current research [133,138–143]. For instance, due to high stability and electrical scalability of Si chips, Si PICs and III-V laser chips can be packaged together through flip-chip bonding [140] and wire bonding [143] with precise optical alignments to achieve a stable integrated functional architecture. Despite this, the efforts of researchers to directly prepare on-chip lasers on Si wafers in the fabrication process stage through heterogeneous integration have accelerated in recent years [25,51]. In order to satisfy the requirements of large-scale production, directly integrating III-V materials on Si substrates has become an ideal solution to solve the core light source problem in Si photonics.

The research on integrated III-V lasers on Si substrates has converged to two primary tracks: quantum well (QW) lasers and quantum dot (QD) lasers. QW lasers refers to the semiconductor lasers that use one or more nanometer-thick QW layers to confine carriers for optical gain, while QD lasers utilize nanoscale QDs to confine carriers, providing a lower threshold and improved temperature stability for the optical gain medium. The first is heterogeneous bonding of QW gain on Si substrates to realize DFB/DBR lasers (DFB lasers refer to the single-frequency lasers in which a periodic grating is built into the gain waveguides to provide wavelength-selective feedback, while DBR lasers use separate grating reflectors to achieve broader tuning than DFB lasers), where current efforts prioritize wafer-level yield, low-loss coupling, and thermal control without linewidth and RIN degradation. The second is QD structure on Si, which leverages QD defect tolerance to improve reliability and back-end compatibility, while recent works focus on uniformity, threshold reduction, and aging behavior. Across both tracks, Si-based integrated lasers are trending toward manufacturable, thermally stable sources with tighter interfaces to Si waveguides.

Toward above goals, in 2006, by using direct bonding between AlGaInAs QW structures and Si waveguides, A. Fang et al. realized the first electrically pumped heterogeneous integrated III-V laser on Si working at room temperature [144], with a threshold of 65 mA and a maximum output power of 1.8 mW. Next, in 2008, they demonstrated a heterogeneous integrated III-V/Si DFB laser with a threshold of 25 mA and a maximum output power of 5.4 mW at the working wavelength of 1600 nm [145], and a III-V/Si DBR laser operating at 1596 nm with a threshold of 65 mA and a maximum output power of 11 mW, which is capable of 4 Gbps OOK transmission by direct modulation [146]. The structures of the early heterogeneous integrated III-V/Si lasers above are shown in Fig. 3(a). Meanwhile, in the same year, Intel realized the integration of heterogeneous III-V/Si sampled-grating DBR lasers with III-V EAMs based on the QW integration platform [147]. The threshold current and the output power for the integrated laser are below 50 mA and above 1.0 mA, respectively, while the modulator bandwidth is 2 GHz with 5 dB extinction. Furthermore, in 2013, IMEC realized heterogeneously integrated III-V/Si QW DFB lasers with 14 mW output power around 1550 nm on 220-nm SOI, utilized an ultra-thin divinyl-bis-benzocyclobutene (DVS-BCB) die-to-wafer bonding process [148,149], and has articulated a broader roadmap for heterogeneous Si photonics, underscoring manufacturability and PDK maturation [150]. In 2015, CEA-Leti/III-V Lab reported further progress on III-V/Si laser integration using direct bonding and detailed the associated packaging and process challenges including thermal design, laser arrays and reliability for volume scaling [151].

The invention of Si-based heterogeneous lasers is an example of the cooperation between academia and industry. Around ten years after the advent of heterogeneously integrated III-V/Si lasers, which can be utilized as on-chip light sources, Intel successfully commercialized fully

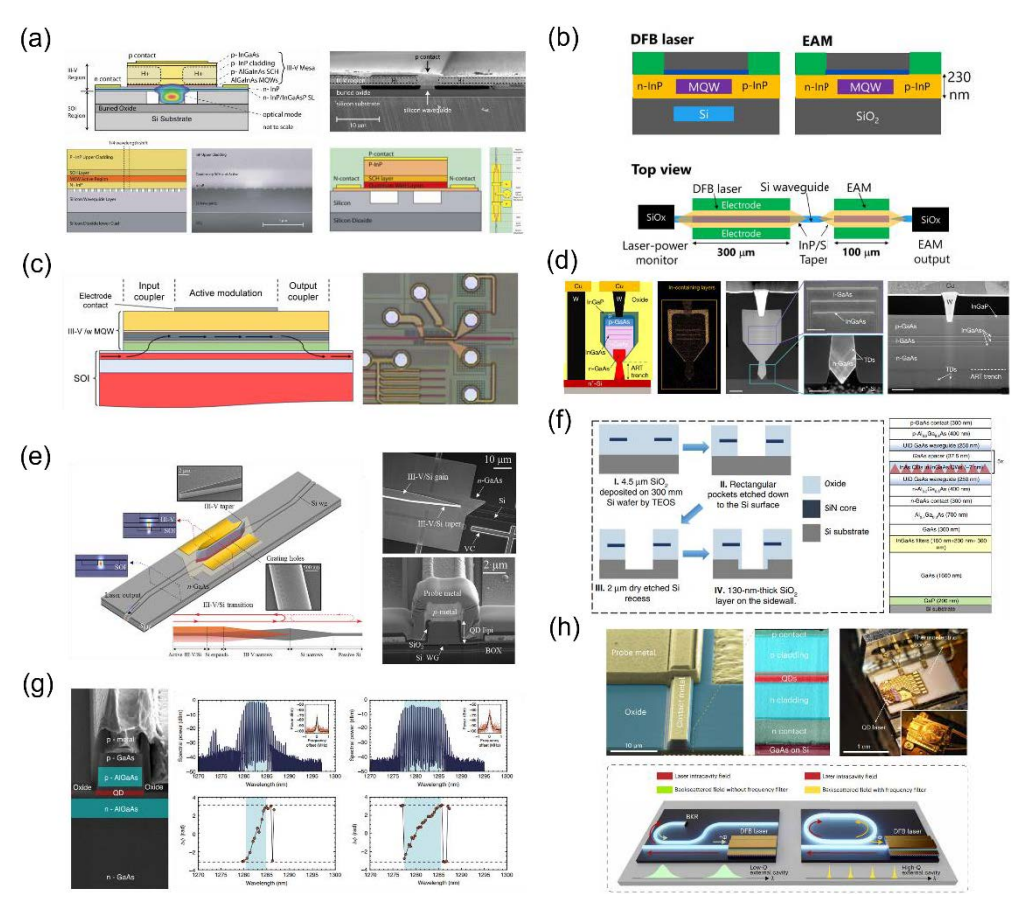


Fig. 3. Integrated lasers on Si. (a) Structures of the electrically pumped heterogeneous integrated III-V/Si lasers at an early stage. Direct bonding is used between QW structures and Si waveguides. Reprinted from Ref. [144-146]. (b) Structure of the heterogenous III-V/Si platform including QW DFB lasers and EAMs. Direct wafer bonding and epitaxial regrowth of InP layers are adopted on the SOI wafer in the fabrication process. Reprinted from Ref. [157]. (c) The high-speed heterogeneous III-V/Si platform on 200 mm SOI wafers. The platform includes on-chip heterogeneously integrated DFB lasers and EAMs together, which can operate in ultrahigh-speed regions. Reprinted from Ref. [159]. (d) The electrically driven III-V laser based on GaAs nano-ridge waveguides and InGaAs QWs. The high-performance devices are fully fabricated on 300 mm Si wafers in CMOS manufacturing line. Reprinted from Ref. [160]. (e) The evanescent QD DFB lasers on Si substrate. The efficient coupling of QD lasers to Si waveguides can be efficiently improved by introducing the wafer bonding step. Reprinted from Ref. [165]. (f) The electrically pumped QD laser grown by MBE on a 300 mm Si wafer. The device structure and Si wafer for growth are shown. Reprinted from Ref. [167]. (g) The broadband QD-MLL with a fast repetition rate. The device can generate both AM and FM combs independently. Reprinted from Ref. [169]. (h) The QD lasers grown directly on Si substrate for self-injection-locking laser coherence under turnkey ECL. The laser structure and turnkey ECL operation schematic are illustrated. Reprinted from Ref. [170].

integrated Si-based transceivers for data center markets [152,153], leading to beyond one billion dollars of revenue [51]. Based on the 300 mm heterogeneous platform, which is capable of both InP-based QW direct bonding process and the fabrication of Si modulators, Intel has

demonstrated multiple Si transceiver products. In 2011, a 50 Gbps (12.5 Gbps  $\times$  4) CWDM Si photonics transmitter using heterogeneously integrated DBR lasers and Si modulator array is achieved in O-band for the first time [154]. After years of development, in 2019, utilizing heterogeneously integrated O-band III-V/Si DFB lasers and high-speed Si MZMs, H. Yu et al. demonstrated a 100 Gbps CWDM4 Si photonics transmitter with 25 Gbps transmission per lane [136]. In 2020, a fully integrated DR4 Si transmitter with 4-channel heterogeneously integrated III-V/Si DFB lasers is realized for 400 Gbps PAM-4 transmission [155]. Furthermore, in 2022, based on 8-channel heterogeneously integrated high-power III-V/Si DFB lasers and Si MZMs, a fully integrated PAM-4  $2 \times$  FR4 and DR8 Si transmitter is achieved for 800 Gbps (100 Gbps  $\times$  8) transmission over 2 km distance, with a working temperature range of  $0 \sim 70^{\circ}$ C [156].

At present, Intel's heterogeneous integration platform still utilizes pure Si modulators based on plasma dispersion effect in the modulation section, which has the advantages of low loss, low cost and large-scale production. Meanwhile, as discussed above, III-V EAMs can also be integrated on the Si substrate to achieve higher transmission rates. In recent years, by introducing multiple III-V QW layer into Si structure, some other industry explorers have also made progress on commercial heterogeneous platforms integrating III-V lasers and EAMs together. In 2023, NTT demonstrated a III-V EAM integrated with a QW DFB laser on Si platform and achieved 112 Gbps OOK with 67 GHz bandwidth [157]. The device structures of the heterogenous III-V/Si platforms are shown in Fig. 3(b). In the fabrication process, direct wafer bonding and epitaxial regrowth of InP layers are adopted on the SOI wafer. Furthermore, in 2025, for 1.6 Tbps and 3.2 Tbps applications for AI-driven markets, Open Light reported a high-speed heterogeneous III-V/Si platform offered through Tower process [158,159], as demonstrated in Fig. 3(c). The platform includes on-chip integrated DFB lasers and EAMs together on 200 mm SOI wafers, which can achieve 256 Gbps OOK, 340 Gbps PAM-4, 375 Gbps PAM-6 and 360 Gbps PAM-8 over 500 m and 6 km SSMF [159], illustrating the potential of III-V/Si platforms for ultrahigh-speed transmissions. Meanwhile, new breakthroughs have also been made for large-scale production of QW lasers in CMOS lines. Recently, in 2025, IMEC reported the electrically driven III-V laser based on GaAs nano-ridge waveguides and InGaAs QWs in Fig. 3(d), which are fully fabricated on 300 mm Si wafers in CMOS manufacturing line [160]. Continuous-wave laser emission around 1020 nm is achieved in 300 devices on a Si wafer, with threshold currents of 5 mA, output powers over 1 mW, laser linewidths of 46 MHz, operation temperature up to 55 °C and the reliability of at least 500 h at room temperature.

With Si-based QW lasers gradually maturing and turning into industrial products, many are now focusing on the new generation of QD lasers on Si platforms. Compared with conventional QW materials, QD lasers are considered to be one promising solution for on-chip Si-based light sources, due to the advantages of low threshold current, high temperature stability, isolator-free operation and reduced sidewall recombination [161,162]. In QD structures, the insensitivity to defects can be enhanced by the high carrier confinement, which will guarantee laser performance even in lattice-mismatched materials, thus increasing the device reliability [163]. Especially, direct epitaxial growth of III-V QD lasers on Si photonic platforms is promising to offer low-cost and scalable PIC systems with multiple functions. In 2019, Y. Wan et al. presented the first tunable single-wavelength QD laser directly grown on Si substrate [164], with a 16 nm tuning range and output powers of 2.7 mW per tuning wavelength. However, the efficient coupling of QD lasers to Si waveguides still needs to be improved. Therefore, on the basis of epitaxial growth of QDs, wafer bonding is introduced to allow QD laser mode fields to overlap with Si waveguides, and the light field is gradually transferred from the QD gain section to the Si waveguide through the taper. In 2021, through optimizing the relationship between QD lasers and Si waveguides, they demonstrated an evanescent OD DFB laser on Si substrate, as shown in Fig. 3(e) [165], with a bandwidth of 13 GHz, a threshold current of 4 mA and a fundamental linewidth of 26 kHz. For the reliability of QD lasers, which is critical for entering practical applications, C.

Shang et al. conducted the high-temperature lifetime test of QD lasers grown directly on Si substrate for the data center environment [166]. By reducing threading dislocation densities and removing misfit dislocations, QD lasers operating in O-band exhibit reliability at 80°C, with an extrapolated lifetime over 22 years after more than 1200 h of constant current stress. Next, in 2022, they realized an electrically pumped QD laser grown by molecular beam epitaxy (MBE) on a 300 mm patterned Si wafer in Fig. 3(f) [167]. The device can achieve continuous wave lasing to 60 °C and a maximum double-side output power of 126.6 mW at 20 °C. Furthermore, for the QD-MLL, which can generate optical comb effectively for multi-wavelength communications [168], in 2023, B. Dong et al. presented a broadband QD-MLL with a fast repetition rate of 60 GHz, which can generate both amplitude-modulated (AM) and frequency-modulated (FM) combs independently [169]. After optimizing the cavity design, the maximum 3-dB bandwidth of 2.2 THz (12.1 nm) can be achieved for the proposed QD-MLL. The device structure together with comb generation are illustrated in Fig. 3(g). For external-cavity locking (ECL) (stabilizing a laser by feeding back an external cavity resonance to narrow the linewidth, reduce phase noise, and improve wavelength stability), in 2024, they demonstrate high-performance QD lasers grown directly on Si substrate in Fig. 3(h), which can achieve self-injection-locking laser coherence under turnkey ECL [170]. The laser exhibits a narrow linewidth of 16 Hz under ECL, with an improved frequency noise compared to conventional QW lasers.

The commercialization of QD lasers is in progress, similar to QW lasers in the past, and Quintessent is a prominent representative explorer in this area. For AI-driven market requirements, Quintessent is developing efficient and reliable QD lasers for DWDM sources in optical systems [171]. Heterogeneously QD lasers are integrated on 200 mm Si wafers with Tower Si photonics platform, and lasers are hermetically sealed under the wafer surface. The lasers can achieve high output power of 10 mW, with operating temperature up to 100 °C. For the reliability testing, the QD lasers showed no obvious performance degradation after 2000h aging at  $2.5 \times$  operating current density and high temperature of 80 °C. Meanwhile, for QD comb lasers, which can be used as multi-wavelength sources for WDM transmissions, 8 comb lines are available currently within a 3 dB fluctuation range, with a frequency spacing of 100 GHz, a single-wavelength lowest power of 8 dBm, a RIN below -147 dBc/Hz and a wall plug efficiency above 25%. Also, the target of 200 GHz frequency spacing is in progress. For the future path, based on high-performance OD lasers, Quintessent's vision is to achieve a heterogeneously integrated optical engine, with transmissions up to 128 Gbps × 32 wavelengths, bandwidth per fiber up to 4.1 Tbps, bandwidth density up to 4.0 Tbps/mm (edge) and 415 Gbps/mm<sup>2</sup> (areal), power consumption below 0.5 pJ/bit as well as transmission reach to 2 km.

Si is the preferred stable material for photonics integration due to the low-cost and large-scale production potential, and the system functionality has already been proven in numerous Si photonics research. The development of on-chip lasers based on Si is the key point to achieve fully integrated Si-based photonic systems, especially for AI applications. The stability and high electrical scalability of Si photonic chips provide the natural advantage in hybrid integration with prefabricated laser chips. More importantly, Si wafers can be adopted as a prominent substrate to develop heterogeneous integration technology for multiple materials including III-V gain sections for lasing. Heterogeneously integrated III-V lasers have been the research focus in Si photonics over the years, and the successful demonstration of on-chip Si-based light sources has directly led to the commercialization of Si photonic products. It is believed that with the advancement of fabrication process, Si-based heterogeneously integrated lasers will achieve continuous progress both in performance and mass production, thus implanting new evolutions into the field of Si photonics.

#### 3.2. Integrated III-V lasers on SiN

In recent years, SiN material has received continuous attention in the field of integrated photonics due to the advantages of ultra-low transmission loss, wide transparent window, high temperature stability and CMOS compatibility [172–175]. Ultra-low loss SiN optical waveguides provide a favorable platform for photonic systems with multiple functions including communications, microwave photonics, sensing, signal processing, nonlinear optics and quantum physics [176–178]. Although SiN material does not have the conditions for luminescence either, benefiting from the ultra-low loss characteristics of SiN waveguides, the laser resonators fabricated on SiN platforms can achieve lower noise and longer photon lifetime [53,179].

Because SiN provides no native gain, integrated lasers on SiN primarily combine III-V gain with ultra-low-loss SiN resonators to form external-cavity or self-injection-locked lasers. Recent work has moved from proof-of-concepts to foundry flows, emphasizing bonding interfaces, low-loss routes, high-Q resonators, and stable narrow-linewidth operation. Multi-wavelength operation increasingly exploits SiN microresonators, such as comb-based carriers, and the pump remains an integrated III-V laser, while key bottlenecks for integrated SiN laser systems are coupling efficiency, thermal drift, and packaging-induced issues. Overall, SiN is consolidating its low-loss platform role for low-noise narrow-linewidth and multi-wavelength integrated laser sources.

There are also two methods to integrate III-V lasers with SiN platforms: hybrid integration and heterogeneous integration. Hybrid integration means using packaging techniques to assemble integrated lasers on III-V substrate with PICs on SiN substrate together to construct photonic systems with various functions [53]. In 2019, C. Xiang et al. reported hybrid lasers based on a gain chip and a SiN PIC with Bragg gratings [180], achieving a fixed wavelength of 1544 nm with an output power of 24 mW and a narrow linewidth of 320 Hz. In 2020, Y. Fan et al. realized a hybrid integrated laser based on an InP gain chip and SiN multi-ring-resonator chip through a low-loss single roundtrip feedback circuit [181], with a narrow intrinsic of 40 Hz and an output power of 23 mW and a 70 nm spectra in 1550 nm wavelength range. In the same year, J. Li et al. demonstrated a hybrid laser based on a III-V DFB laser and a SiN subwavelength hole defect assisted microring reflector PIC, shown in Fig. 4(a) [182], with a narrow intrinsic linewidth of 34.2 Hz, a high output power of 11.7 dBm and a large side mode suppression ratio (SMSR) of 50 dB in C-band. It can be seen that, based on low-loss SiN PICs, hybrid narrow-linewidth high-power integrated lasers can be realized for around 1550 nm communication wavelength region. For shorter wavelengths and multiple functions beyond communications, in 2022, A. Siddharth et al. reported a hybrid integrated laser based on a GaN-based laser diode and a SiN microresonator PIC in Fig. 4(b) [183], which can operate at short wavelength around 410 nm in the near-ultraviolet region, and the optical phase noise can be reduced effectively by self-injection locking of the laser to the high-Q resonator on SiN PIC.

For heterogeneous integration, which refers to integrating different materials including III-V and SiN layers on the single substrate, the micro-transfer printing process and wafer bonding technology can be used on SiN platforms. For micro-transfer printing, in 2021, S. Cuyvers et al. demonstrated a heterogeneously integrated III-V/SiN MLL by micro-transfer printing process, shown in Fig. 4(c) [184]. By using long low-loss SiN external cavities, the laser exhibits a narrow line spacing of 755 MHz, an optical linewidth below 200 kHz and a RF linewidth of 1 Hz. Similarly, by using micro-transfer printing, compact vertical-cavity surface-emitting laser (VCSEL), which has the advantages of low cost and high energy efficiency [185], can be integrated on the SiN platform to achieve the working wavelength of 850 nm with mW-level power consumption [186]. For wafer bonding technology with greater integration advantages, the main difficulty is the large refractive index mismatch between III-V gain materials and SiN low-loss waveguide [53]. Multilayer heterogeneous integration can be utilized to mitigate this issue, in which an intermediate Si layer is introduced to realize the transition of mode refractive

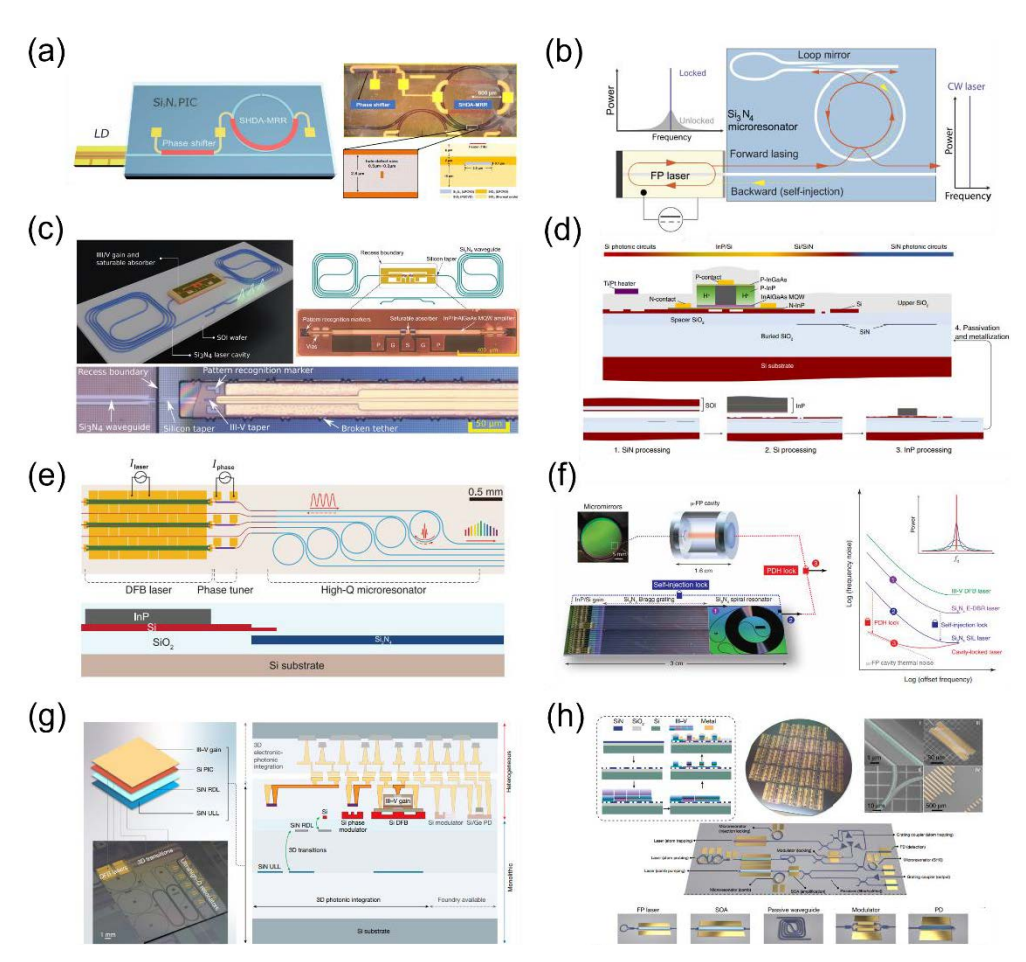


Fig. 4. Integrated lasers on SiN. (a) The hybrid laser based on a III-V DFB laser and a SiN PIC. The subwavelength hole defect assisted microring reflector structure is fabricated on the SiN platform to enhance the laser performance. Reprinted from Ref. [182]. (b) The hybrid integrated laser based on a GaN-based laser diode and a SiN PIC. The laser can operate at short wavelength around 410 nm, and the optical phase noise can be reduced by self-injection locking of the laser to the resonator on the SiN PIC. Reprinted from Ref. [183]. (c) The heterogeneously integrated III-V/SiN MLL by micro-transfer printing process. The integrated passively MLL has a narrow sub-GHz comb line spacing by using long low-loss SiN external cavities. Reprinted from Ref. [184]. (d) The electrically driven heterogeneously integrated III-V/Si/SiN multilayer laser. The heterogeneous laser is fabricated using wafer bonding, with the advantages of high power, narrow linewidth and low noise. Reprinted from Ref. [188]. (e) The heterogeneously integrated laser soliton microcombs based on InP/Si laser and low-loss SiN resonators. Single soliton microcombs can be generated by electrically controlling the relative optical phase between the laser and resonator. Reprinted from Ref. [189]. (f) The integrated laser system with a narrow linewidth of 1 Hz. The system is based on the heterogeneously integrated SiN-based lasers and compact FP cavities, where key components are fabricated lithographically on planar substrates. Reprinted from Ref. [190]. (g) The device structure of the ultralow-noise isolator-free integrated laser. Based on the three-dimensional integration, the III-V/Si/SiN heterogeneous integrated laser is separated into four functional layers including a III-V gain layer, a Si PIC layer, a SiN RDL and a SiN ULL layer. Reprinted from Ref. [191]. (h) The heterogeneously integrated SiN platform operating at sub-micron short wavelengths. The lasers, amplifiers, photodetectors, modulators, and passive waveguides are demonstrated on the heterogeneous platform. Reprinted from Ref. [197].

index and implement multi-mode conversions between III-V gain region and SiN resonators. In 2020, C. Xiang et al. reported a novel heterogeneous III-V/Si/SiN structure to realize lasing in a fully integrated low-loss SiN-based external cavity, with excellent temperature stability, narrow linewidth output and low phase noise [187]. The device structure is constructed by bonding a SOI wafer and an InP wafer to a SiN wafer in order. In 2021, by further optimizing the device design, they demonstrated an electrically driven III-V/Si/SiN multilayer heterogeneous integrated laser in Fig. 4(d) [188], which is fabricated using wafer bonding, with a high power more than 10 mW, a fundamental linewidth narrower than 1 kHz and a RIN lower than −150 dBc/Hz. By self-injecting the integrated on-chip laser into an ultrahigh-Q SiN resonator, a frequency noise reduction of 30 dB and a corresponding linewidth of 3 Hz can be realized, and optical frequency combs can be generated directly due to the high laser power under Fabry-Pérot (FP) working mode and the reduced coupling loss brought by heterogeneous integration. In the same year, they demonstrated heterogeneously integrated laser soliton microcombs based on InP/Si laser and low-loss SiN resonators on the monolithic Si substrate, as shown in Fig. 4(e) [189], with laser frequency noise reduction due to self-injection locking. Single soliton microcombs with a 100 GHz repetition rate can be generated by electrically controlling the relative optical phase between the laser and resonator on chip. For the continued narrowing of linewidth, in 2022, based on the heterogeneously integrated SiN-based lasers as the pump source and compact FP cavities, J. Guo et al. presented an integrated laser system with a narrow 1-s linewidth of 1 Hz and fractional frequency instability below  $10^{-14}$  to 1 s [190], shown in Fig. 4(f), where the key components are all fabricated lithographically on planar substrates. Furthermore, in 2023, C. Xiang et al. demonstrated the ultralow-noise isolator-free lasers by multiple monolithic and heterogeneous processing sequences based on three-dimensional integration structure [191]. The high-performance III-V/Si DFB laser is combined with an ultrahigh-Q SiN resonator, and the III-V/Si/SiN heterogeneous integrated laser is separated into four main functional layers including a III-V gain layer, a Si PIC layer, a SiN redistribution layer (RDL) and a SiN ultra-low loss (ULL) waveguide layer, as shown in Fig. 4(g). After the laser achieves wavelength and phase matching with the SiN microring resonator, the free-running laser is locked to the SiN resonator by self-injection through Rayleigh backscattering. The device with 0.5 dB/m optical loss ULL exhibits ultra-low frequency noise performance with the white noise floor of  $1.7 \,\mathrm{Hz^2 \,Hz^{-1}}$  for the drop port and an intrinsic linewidth of 5 Hz.

Nowadays, with favorable performance and CMOS compatibility for wafer-scale production, the heterogeneous integration based on SiN is being commercialized, and Nexus Photonics is one example in this area [192,193]. Based on the low-loss SiN platform, by integrating a variety of III-V materials (e.g. GaAs, GaN, InP) to extend the wavelength range of operation, many emerging functions beyond communications can be realized [194]. The realization of short-wavelength PICs has the potential in a series novel application such as augmented reality (AR)/virtual reality (VR), visible light communications, atomic physics as well as quantum systems [195], and these application fields are closely complementary to AI. For instance, AR/VR headsets will generate high-rate visual and inertial data that must be interpreted in real time by on-device AI for multiple functions such as eye/hand tracking, scene understanding and foveated rendering. The heterogeneously integrated GaAs/SiN lasers provide compact, low-RIN, narrow-linewidth and fast-modulated illumination that raises SNR for AI perception and reduces system size, weight and powers, releasing power budget for inference. Beyond sensing and display, the GaAs/SiN-based combs can also serve as the multi-wavelength sources for photonic interconnects and accelerators, linking AR/VR front-ends and AI hardware within low-latency photonic systems. In 2020, H. Park et al. reported electrically pumped heterogeneous GaAs/SiN lasers operating around 990 nm for the first time [196]. Furthermore, in 2022, M. Tran et al. demonstrated a fully integrated heterogenous PIC platform by directly integrating III-V materials with low-loss SiN waveguides on Si wafers, shown in Fig. 4(h) [197]. Multiple photonic devices are shown,

including active components such as lasers, amplifiers, photodetectors, modulators, and passive waveguides at sub-micron short wavelengths. Especially, a heterogeneously integrated tunable laser with narrow linewidth of 2.8 kHz and RIN less than  $-155\,\text{dB/Hz}$  at 980 nm operation wavelength, which is beyond the bandgap energy of Si, is achieved by the combination of short-wavelength GaAs material with SiN external cavities. Next, in 2023, Z. Zhang et al. has improved the heterogeneous SiN platform and extended the laser operating wavelength to 780 nm by using high-bandgap GaAs materials [198], while remaining the working temperature up to  $110^{\circ}\text{C}$ . For even shorter wavelengths around 460 nm, this can be achieved by heterogeneously integrating electrically pumped GaN-based sources on the SiN platform [192], while longer wavelengths around 1550 nm can be realized by integrating InP materials [193]. The integrated lasers operating from short-wavelength to long-wavelength region demonstrate the great potential including process compatibility and functional scalability of the heterogeneous SiN platform.

SiN is an excellent platform for photonic integration with ultra-low loss and CMOS compatibility, and a variety of multifunctional photonic systems based on SiN platforms have been demonstrated. Although SiN cannot emit light by itself, its low-loss advantage enables the integrated III-V lasers on SiN platforms to exhibit a series of advantages such as narrow linewidth and low noise. By hybrid integration, the III-V gain chip can be combined with functional SiN PIC to realize the performance enhancement of the laser. Furthermore, for heterogeneous integration, which has made a lot of impressive progress nowadays, III-V lasers can be integrated on the low-loss SiN platform directly through micro-transfer printing and wafer bonding technology. Meanwhile, by integrating different III-V materials on SiN, multiple lasing bands in the fully integrated on-chip systems can be achieved effectively to satisfy various application requirements.

## 3.3. Integrated III-V lasers on TFLN

With the excellent EO performance, low transmission loss, strong second-order nonlinearity and wide transparent window, TFLN material, which can be fabricated on SOI substrate, has become an emerging PIC platform with high comprehensive performance and has made a series of progress in the fields of high-speed transmission, microwave photonics, signal processing, etc [76,77,83,85]. Therefore, the development of integrated lasers on TFLN, especially electrically pumped ones, has become the next step of photonic system integration. With the TFLN research increasing, researchers have proposed a variety of laser integration methods, including hybrid and heterogeneous integration.

On TFLN platforms, integrated lasers rely on III-V gain combined with LN microresonators to realize optical sources, benefitting from fast EO tuning inherent to LN. Current emphasis is on hybrid co-packaging and heterogeneous integration of III-V dies to LN waveguides with low parasitic reflections, while addressing photorefractive, thermal effects and wafer-level screening of bonded interfaces to raise yield, reliability and long-term stability. Considering the prominent modulation properties of LN, the trend is toward EO-tunable, narrow-linewidth heterogeneously integrated III-V lasers with LN PICs, especially for transceiver applications.

Currently, most approaches for integrating III-V lasers with LN PICs are to package prepared III-V chips with LN PICs through hybrid integration. In 2021, Y. Han et al demonstrated a hybrid electrically pumped III-V/LN laser by coupling an InP-based gain chip with a TFLN PIC, in which a Vernier filter of two resonators is used to select the laser wavelength [199]. The hybrid laser has a wavelength range of 36 nm in O-band, with a maximum power of 2.5 mW. In 2022, A. Shams-Ansari et al. demonstrated a hybrid integrated electrically pumped laser on TFLN platform, with 60 mW optical power into the TFLN waveguides, shown in Fig. 5(a) [200]. By flip-chip bonding an InP-based DFB laser with a prefabricated TFLN PIC, a high-power transmitter integrated with a 50 GHz modulator is realized. Particularly, the support structures are added for the DFB laser to provide better mechanical stability in the flip-chip bonding process.

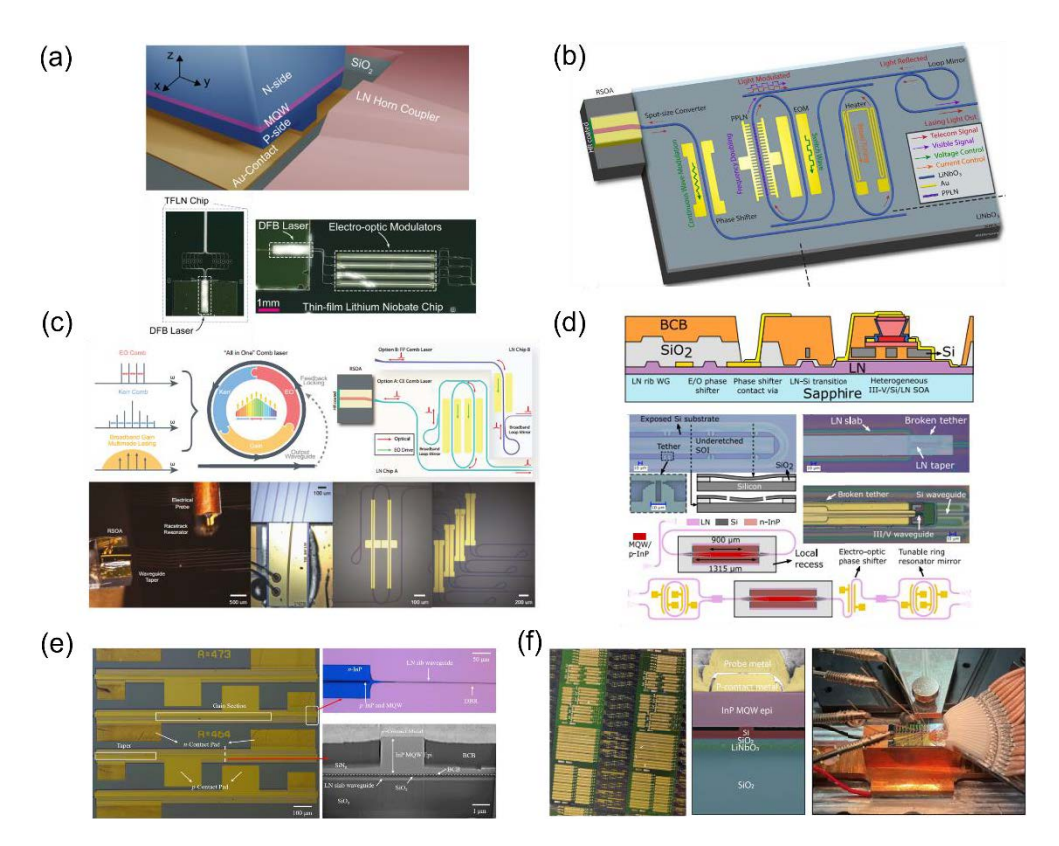


Fig. 5. Integrated lasers on TFLN. (a) The hybrid integrated electrically pumped III-V laser on TFLN platform. An InP-based DFB laser is integrated with a prefabricated TFLN PIC by flip-chip bonding process. Reprinted from Ref. [200]. (b) The integrated Pockels laser based on a hybrid integrated III-V/LN structure. By introducing the EO effect into the laser on TFLN platform, an ultra-high frequency modulation is realized. Reprinted from Ref. [201]. (c) The on-chip mode-locked microcomb laser based on hybrid integration between III-V gain chip and TFLN PIC. The laser can directly emit mode-locked microcomb on demand with robust turnkey operation. Reprinted from Ref. [203]. (d) The heterogeneously integrated electrically pumped lasers and amplifiers on TFLN by micro-transfer printing process. The optical amplifiers, multimode ring lasers, and single-mode tunable lasers are demonstrated on the heterogeneous platform. Reprinted from Ref. [204]. (e) The heterogeneously integrated InP-based DBR laser on TFLN through dielectric adhesive bonding with BCB layer. The optical field is coupled from the active region to the TFLN waveguide based on a multi-section spot size converter. Reprinted from Ref. [206]. (f) The heterogeneously integrated InP-based DFB laser on TFLN through direct wafer bonding. The optical micrograph and SEM image of the heterogeneously integrated laser are shown. Reprinted from Ref. [208].

Simultaneously, based on hybrid integration, some lasers can achieve improved functionality by introducing novel structures. In 2022, by introducing the EO effect into the semiconductor laser on TFLN, M. Li et al. designed an integrated Pockels laser using a hybrid integrated III-V/LN structure, as demonstrated in Fig. 5(b) [201]. An ultra-high frequency modulation of 2 EHz/s and fast switching at 50 MHz are realized, and the infrared and visible frequencies can both be generated through second-harmonic frequency conversion process. In 2023, J. Ling et al. presented a hybrid integrated light source for high-coherence near-visible emitting, with a short-term linewidth of 4.7 kHz and a converted power over 2 mW [202]. The wavelength

conversion and coherence increase by self-injection locking are combined with a TFLN nonlinear resonator, which is pumped by a III-V DFB laser chip, and the conversion efficiency and the output power can be increased by heterogeneous integration. Furthermore, for on-chip microcomb generation, they demonstrated an on-chip MLL based on hybrid integration between III-V gain chip and TFLN PIC in Fig. 5(c) [203], achieving microcomb with comb linewidth of  $600\,\mathrm{Hz}$  and frequency tuning rate of  $2.4\times10^{17}\,\mathrm{Hz/s}$ , on demand with robust turnkey operation.

In recent years, with the enhancement of fabrication processes, heterogeneous integration technology on TFLN has also made significant progress, including micro-transfer printing. dielectric adhesive bonding, and direct wafer bonding. In 2021, C. Beeck et al. reported electrically pumped lasers and amplifiers heterogeneously integrated on TFLN by developing a back-end micro-transfer printing process, shown in Fig. 5(d) [204]. The optical amplifiers, multimode ring lasers, and single-mode tunable lasers are fabricated based on the heterogeneous platform. Furthermore, in 2024, by utilizing the micro-transfer printing process, NTT realized the heterogeneous integration of electrically pumped InP-based lasers and achieved 128 Gbps OOK transmission with a MZM on the TFLN platform [205]. In 2023, X. Zhang et al. reported a heterogeneously integrated InP-based DBR laser on TFLN through dielectric adhesive bonding with a benzocyclobutene (BCB) layer [206], where the optical field from the active region is coupled to the TFLN waveguide by a multi-section spot size converter, achieving a threshold current of 80 mA and an output optical power of 1 mW. The device structure and images of the heterogeneously integrated laser are shown in Fig. 5(e). For directly wafer bonding, in 2024, T. Morin et al. presented a heterogeneous GaAs-based integrated laser on a TFLN wafer [207], which operates in the near-infrared band with multi wavelengths. In the same year, M. Li et al. reported a heterogeneously integrated InP-based DFB laser on TFLN working in C-band through direct wafer bonding of III-V thin film, TFLN layer and SOI wafer in Fig. 5(f) [208], with an optical power of 16 mW, a SMSRof 50 dB and an intrinsic linewidth of 22.0 kHz by self-injection locking. Furthermore, in 2025, based on the heterogeneous DFB laser, they demonstrated a high-speed transmitter integrated with a 50 GHz MZM on TFLN, achieving 10 Gbps OOK transmission with clear open eyes [209].

TFLN has been proven to be an excellent photonic integration platform with high functional scalability, while the introduction of integrated lasers will significantly improve the system integration level. Integrating III-V chips with TFLN PICs to form a single system through hybrid integration can achieve energy efficiency and functionality improvements compared to traditional bench-top laser schemes. Furthermore, by developing heterogeneous laser integration in fabrication process, the complete functional systems can be prepared based on the heterogeneous TFLN platform. Especially, with the improvement of direct wafer bonding technology, based on the inherent prominent EO properties of TFLN, multiple functions such as intracavity frequency conversion, optical signal processing, optical metrology and quantum photonics can be realized using fully integrated on-chip photonic TFLN systems.

Across different integration schemes, commercial scalability is closely related to process maturity and testability. Hybrid integration of III-V laser chips with Si/SiN/TFLN PICs is already widely adopted, with packaging and co-testing flows becoming increasingly stable and moving toward high-volume manufacturing. In parallel, heterogeneous integration of III-V gain with these scalable platforms is attracting attention and delivering important breakthroughs, since it enables wafer-level integration and compact coupling, on the basis of tightly controlled bonding yield and thermal control budgets. For different platforms, Si is led by mature QW lasers so far, with next steps focused on lowering coupling loss, suppressing parasitic reflections, and improving thermal management; meanwhile, QD-on-Si, with superior temperature robustness, is progressing toward manufacturability. For ultra-low-loss transmission, SiN is consolidating its role as the external cavity for narrow-linewidth low-noise lasers, where engineering effort centers on coupling efficiency, thermal drift, and long-term stability. As for TFLN, which has been widely developed

because of the prominent EO modulation capability, it leverages fast EO tuning by coupling III-V gain to LN resonators, and current priorities include compact butt-coupling or bonding, robust thermal management, and wafer-level screening to ensure reliability. Looking ahead, the pathway from laboratory prototypes to deployable AI hardware is gradually defined. Key approaches include achieving on-chip isolation or inherent backreflection tolerance, suppressing low-frequency noise that constrains coherent transmission and analog computing, delivering wafer-level yield with large channel redundancy, and standardizing process-compatible, low-loss coupling and assembly across Si/SiN/TFLN platforms. Sustained progress along these aspects will directly improve the system bandwidth and energy efficiency, providing a clear route to commercially scalable integrated lasers for AI systems.

# 4. Application of integrated lasers for Al

In AI photonic systems, the integrated laser is the core optical source that enables a wide range of applications. Here we list optical interconnections, optical neural networks, and LiDAR as representative cases, across Si/SiN/TFLN platforms and III-V gain co-integrated with these PICs. For optical interconnections (IM/DD and coherent), laser-centric limits are governed by noise, stability, and the interface between lasers and PICs. Multi-level eye openings in IM/DD links are primarily limited by RIN and mode-partition noise, which will set the available SNR, while maintaining stable output power prevents penalties from additional loss as lane counts grow. In coherent links, the linewidth and frequency noise of the laser determine the required phase tracking and OSNR margin. Since the on-chip cavity is susceptible to frequency drift and parasitic reflections from the PIC, the light source must be able to withstand backreflections or be isolated. In optical neural networks, analog multiply-accumulate (MAC) operation accuracy is sensitive to RIN/noise and slow drift that triggers recalibration. Therefore, light sources must provide low noise, narrow linewidth, stable power, and channel-to-channel uniformity, with laser-PIC interfaces engineered for low insertion and minimal parasitic reflections to support arrayed carriers without mode hopping or additional drift. As for LiDAR systems, the dominant constraints are coherence and tunability. The linewidth and phase/frequency noise dictate coherence length and ranging SNR, while chirp linearity, sweep bandwidth, and shot-to-shot repeatability bound velocity and range accuracy. Meanwhile, wavelength stability and favorable SMSR will reduce leakage and crosstalk for long-term reliable coherent detections.

#### 4.1. Optical Interconnections

The rapid development of AI has brought about an exponential growth in the data transmitted and processed, which has put forward increasingly higher requirements on the bandwidth, capacity, power consumption of optical interconnections and communications [9]. Developing high-bandwidth, low-power-consumption optical interconnections within computing centers is key to enabling low-latency AI models [210]. Therefore, based on the miniaturization advantages brought by integrated lasers, designing high-density optical interconnections is the primary application path of integrated lasers for AI.

Intel is a representative industry explorer, which has been working in the field of optical interconnection technology over the years [58], especially for on-chip integrated lasers on SOI platforms. As discussed above, based on heterogeneously integrated QW lasers and MZMs on Si platforms, Intel has demonstrated several commercial transceiver products for data center markets. However, Si MZMs still occupy a relatively large area for large-scale photonics systems. To solve this issue, Intel has conducted a series of work on the integration between Si MRMs with on-chip lasers in recent years, which has the advantages of compact footprint and low power consumption. In 2020, H. Li et al. presented a hybrid integrated 112 Gbps PAM-4 Si photonics transmitter with an on-chip integrated laser, a Si MRM and a co-packaged integrated 28 nm CMOS driver, shown in Fig. 6(a) [211]. In 2023, X. Wu et al. demonstrated a dual-polarization single-wavelength

transceiver operating at 320 Gbps PAM-4 transmission [212], including a hybrid integrated III-V/Si DFB laser, Si MRMs, photodetectors, and polarization DeMUX with automatic control. Furthermore, in 2024, by introducing MRM structure into MZMs, they reported an integrated Si photonic transmitter including an on-chip DFB laser and a push-pull ring-assisted MZM [213]. High-speed transmission of 224 Gbps PAM-4 is achieved using a 1.8 Vppd differential driving voltage, with a transmitter and dispersion eye closure quaternary (TDECQ) of 1.25 dB, while no obvious TDECQ degradation is found over 1-km SSMF. For next-generation high-performance QD lasers, in 2025, D. Huang et al. demonstrated QD lasers heterogeneously integrated with

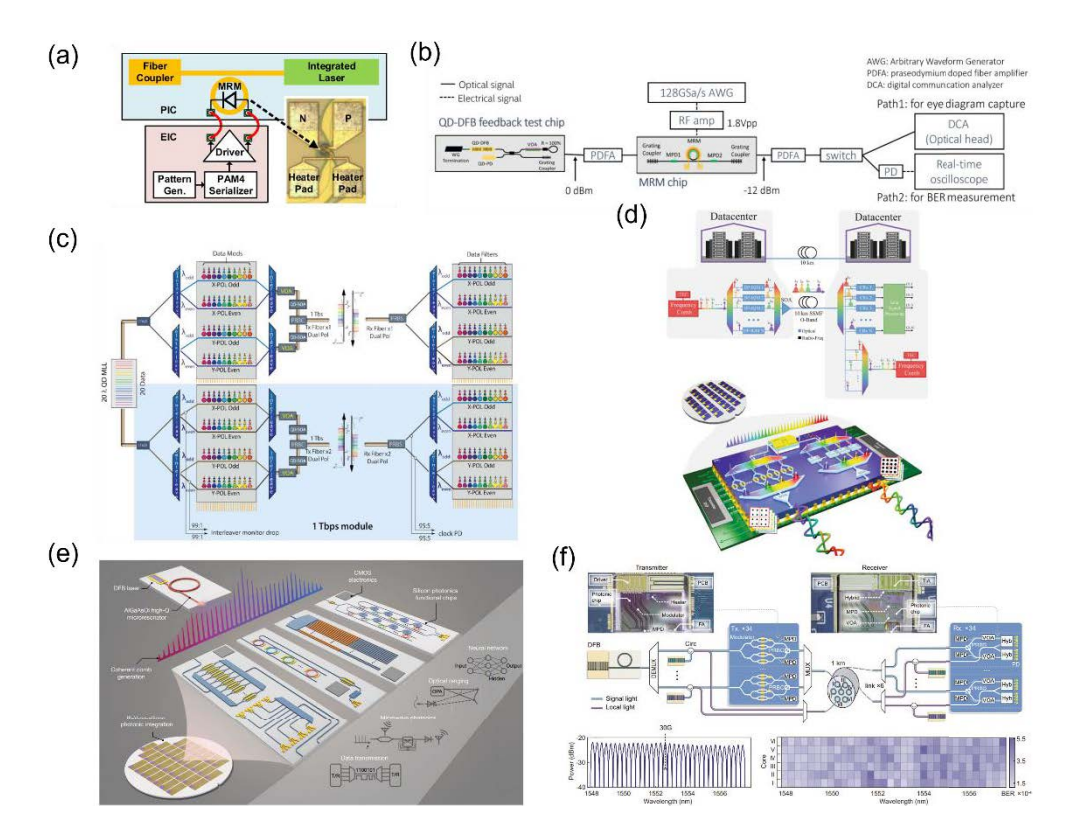


Fig. 6. Optical interconnections with integrated lasers. (a) System architecture of the hybrid integrated Si photonics transmitter. An on-chip integrated laser, a Si MRM and a co-packaged driver are included. Reprinted from Ref. [211]. (b) The experimental system of the isolator-free data transmission of a QD laser and a Si MRM. The fabricated QD laser has a high feedback tolerance, thereby it is unnecessary to adopt the isolator when combing with a Si MRM. Reprinted from Ref. [214]. (c) Architecture of the low-power and high-capacity optical system for IM/DD interconnections based on a QD-MLL source. The Tbps-level optical link with a total energy consumption of sub-pJ/bit is achieved. Reprinted from Ref. [127]. (d) Architecture of the coherent optical link for high-capacity and long-distance transmission based on QD-MLLs. Two independent comb lasers are adopted as sources, one for the carrier and one for the LO. Reprinted from Ref. [130]. (e) Microcomb-driven Si photonics systems. By combining an optical microcomb source directly pumped by the DFB laser with Si photonic chips together, several functions including data transmission, microwave photonics, optical ranging and neural networks can be achieved. Reprinted from Ref. [128]. (f) Architecture of the coherent communication system based on an optical microcomb source. The spectra of all 34 modulation channels and BERs of 34 wavelengths within 6 fiber cores are also shown. Reprinted from Ref. [131].

300 mm Si photonics for the first time [214]. The fabricated laser has a high feedback tolerance, so it is unnecessary to use the isolator when combing with a Si MRM. The isolator-free optical link in Fig. 6(b) achieves 128 Gbps PAM-4 signal transmission and illustrates the potential of QD lasers integrated with pure Si modulators for 300 mm Si photonic platforms.

Furthermore, the QD-MLL, which can generate comb using a single laser, is a good light source choice for multi-wavelength optical interconnections, especially for WDM applications. In 2019, S. Liu et al. demonstrated a total data capacity of 4.1 Tbps based on a low-noise high-channel-count 20 GHz passively QD-MLL grown on a Si substrate [215]. Among the total comb lines of the laser, 64 wavelength channels are utilized to achieve a 64 Gbps PAM-4 transmission. In 2022, S. Pan reported a two-section QD-MLL which can generate an optical comb with a fundamental repetition rate of 100 GHz [216]. The laser has a low RIN value less than -134 dB/Hz from 100 MHz to 10 GHz and 128 Gbps PAM-4 transmission is achieved based on 7 comb wavelengths in O band. In 2024, A. Netherton et al. proposed a low-power and high-capacity optical system for short-reach IM/DD interconnections by adopting a OD-MLL source, with power consumption of only sub-pJ/bit, as demonstrated in Fig. 6(c) [127]. The packaged 20-wavelength QD-MLL comb source has a free space wall plug efficiencies up to 17%, uniform power distribution on each line, and a RIN per line of -151 dBc/Hz at 10 GHz offset. For each PIC, 1 Tbps optical link with a bandwidth density of 5.3 Tbps/mm<sup>2</sup> and a total energy consumption below 0.4 pJ/bit is achieved. Recently, in 2025, based on one QD-MLL and the Si MRM array, J. Chen et al. demonstrated an 8 × 100 Gbps transmitter in O-band based on 8 comb lines, with a total energy efficiency of 1.66 pJ/bit [217]. These interconnection systems illustrate the impressive low-power potential for QD-MLL-based optical links. Meanwhile, although the low-cost and easy-to-implement IM/DD configurations are regarded as technology routes in data centers currently, the coherent transmission solution is still a competitive choice for long-distance optical links, especially in data center to data center scenarios. In 2022, G. Liu et al. a total data capacity of 12.5 Tbps 16-QAM transmission over 100-km single mode fiber in C-band based on a QD-MLL and 56 wavelength channels are utilized in the transmission systems [218]. In 2024, S. Bernal et al. demonstrated a coherent optical link based on QD-MLLs for high-capacity and long-distance transmission, shown in Fig. 6(d) [130]. Two independent free running comb lasers are adopted as sources, one for the carrier and one for the local oscillator. Based on the comb architecture, a 12.1 Tbps system is achieved by using 26  $\lambda$ s with 0.47 Tbps/ $\lambda$ , over a 10 km single mode fiber in O-band.

Simultaneously, based on optical resonators, using integrated III-V DFB laser chips as pumps to generate optical frequency combs is also an effective way to construct stable multi-wavelength light sources, which is significant to achieve high-capacity parallel optical transmission. The frequency spacing of the optical comb sources is based on the self-locking mode in the cavity and depends on the free spectral range of the passive resonator. Therefore, the stability of microcomb solution exceeds that of the laser array, which only needs to stably control a single on-chip laser and a passive optical resonator, avoiding the increase in system complexity and energy consumption as the array scale expands. In recent years, using on-chip DFB lasers as pump sources to generate optical frequency combs for interconnect communications has been widely studied, for both IM/DD and coherent systems. In 2022, H. Shu et al. demonstrated a microcomb-driven Si photonic transceiver for PAM-4 WDM transmission, combining the microcomb technology and Si photonics together [128]. The proposed system architecture is illustrated in Fig. 6(e). A dark-pulse microcomb can be generated by an aluminum gallium arsenide (AlGaAs) high-Q resonator, which can be directly pumped by an on-chip DFB laser. In the integrated DFB pump scenario, 64 Gbps PAM-4 transmission can be achieved on one channel, leading to a total data capacity of 448 Gbps. For SiN resonators, in 2022, Y. Geng at al. reported WDM optical communications using an integrated SiN perfect soliton crystal as the multi-channel laser source pumped directly by a DFB laser chip [219]. The power of integrated Kerr soliton

microcombs can be enhanced by perfect solution crystals for modulation without preamplification, and 80 Gbps 16-QAM as well as 44 Gbps PAM-4 data transmissions are demonstrated for 10 km and 50 km distances. Furthermore, the phase-related DSP consumption can be reduced greatly by using comb solutions compared to traditional laser schemes in coherent systems. In 2024, X. Zhang et al. presented a high-coherence parallelization strategy by using a self-injection locked microcomb to injection lock on-chip DFB lasers [131]. The SiN microresonator is adopted for comb generation and an on-chip gain of 60 dB with no degradation in coherence is obtained. The proposed coherent system, which is shown in Fig. 6(f), demonstrated a total data capacity beyond 60 Tbps by using DP-32-QAM operating at 150 Gbps in 34  $\lambda$ s within 6 fiber cores. From the above representative works, it can be seen that generating high-quality optical combs by using integrated lasers as direct pumps of optical resonators is also an effective way to construct multi-wavelength light sources based on a single laser.

Optical interconnection is the direct and effective application of integrated lasers for data growth in the AI era. Integrated lasers have advantages in reducing energy consumption and costs of interconnection systems, while increasing integration density significantly. Based on different types of integrated lasers, various schemes have been proposed for short-distance IM/DD interconnections and long-distance coherent communications. Considering the application value of optical interconnections for AI, based on the highly scalable Si photonic platforms, integrating lasers and transmission links on a single chip through heterogeneous process to construct large-scale multi-wavelength high-speed optical interconnection systems, is the key development direction of integrated lasers in the future.

#### 4.2. Optical neural networks

With the development of deep learning, when dealing with large-scale AI tasks, traditional electronic computing can no longer continue to achieve effective performance improvements due to the bottlenecks caused by speed and power consumption [220]. Therefore, optical computing, which directly uses photons for signal processing, has attracted widespread attention as a promising alternative technology path [221]. Relying on the inherent high-bandwidth and low-energy-consumption characteristics of photons, the optical computing based on optical neural networks is expected to significantly reduce latency and energy consumption in the data processing process, thereby achieving performance improvements and providing new solutions for next-generation AI hardware [222]. The core concept of optical neural network is to use specific optical devices to implement key mathematical operations involved in neural networks from the traditional electronic field to the optical domain, such as vector-matrix multiplication, convolution operations, and nonlinear activation functions. According to the light field control components and the working mechanisms in photonic neural networks, a variety of physical implementation architectures have been proposed [223], demonstrating the advantages of photonic neural networks in computing speed and energy efficiency [224]. The research of optical computing systems originated from free-space optics and now has gradually shifted to integrated photonic chips with the rapid development of optoelectronics [225–227]. However, for most on-chip integrated chip schemes, the light emitters used in practical experiment systems are still based on the traditional bench-top laser equipment [228–232], which limits the integration level and increase energy consumption of the entire optical computing systems.

The utilization of integrated lasers provides an effective solution to minimize the size of optical computing systems, while the low energy consumption can reserve more power budget for the computing unit. Based on this concept, some representative works have been carried out. For example, by adopting the compact VCSEL array, which is an integrated micron-scale and mass-producible integrated laser light source based on III-V elements [185], the optical neural networks exhibit advantages in both compute density and energy efficiency. In 2022, Z. Chen et al. demonstrated a spatial-temporal-multiplexed optical neural network system based on compact

VCSEL arrays [233]. The VCSEL adopted has an efficient EO conversion ( $V\pi = 4 \text{ mV}$ ) and a compact footprint (<0.01 mm²), which provides the basis for efficient and compact integrated solution. The proposed system exhibits a computing density of 6 TOPS/mm²/s and an energy efficiency of 7 fJ/OP (TOPS: 1 trillion of operations per second). A more scalable option that can be combined with a Si-based platform in the future is the DFB laser scheme [234]. In 2024, X. Guo et al. presented an integrated neuromorphic photonic scheme for time-delayed optical reservoir computing based on a 4-channel DFB laser array with optical feedback and injection [235]. With the size of the DFB array increasing, the ability to handle complex tasks will be further improved. Furthermore, in 2025, Z. Dai et al. optimized the photonic reservoir computing system based on a novel DFB laser with saturable absorber (DFB-SA laser), leading to faster response time with lower power consumption [236].

With the development of on-chip optical computing systems, in large-scale optical neural networks for complex AI tasks, muti-channel laser arrays are required to enhance the system performance [237]. The use of multiple traditional bench-top lasers will limit the overall system integration and energy efficiency, especially compared to single-channel scenarios. Therefore, the adoption of high-performance multi-channel integrated DFB laser modules will mitigate the system power consumption effectively. The system architecture of a representative highly integrated 64 × 64 photonic computing engine is illustrated in Fig. 7(a), which is powered by 4-channel DFB modules [238]. The proposed large-scale system consists of more than 16000 photonic elements for standard linear matrix multiply-accumulate functions, which is capable of computing at a high speed of 1 GHz frequency and a low latency of 3 ns per cycle. Simultaneously, emerging optical frequency comb technology provides an effective way to provide multi-wavelength light sources in on-chip optical neural network systems [239]. Based on an optical microcomb source, a universal optical vector convolutional accelerator interleaving temporal, wavelength and spatial dimensions simultaneously is demonstrated, which can operate at more than ten TOPS [240]. Furthermore, the DFB laser chip can be used as a direct pump for optical microcomb, thereby converting a single wavelength light source into a multi-wavelength light source for optical neural networks, shown in Fig. 7(b) [241,242]. In 2023, B. Bai et al. proposed an integrated photonic processing unit, which utilized an optical convolution accelerator architecture based on the integrated optical microcomb [243]. In the system, an AlGaAs microring resonator is pumped directly by an integrated DFB laser chip to generate the optical microcomb. The on-chip parallel convolution operations can be implemented through a time-wavelength plane stretching method. The integrated computing system combines a Si MZM, a MRR weight bank and delay lines, as demonstrated in Fig. 7(c), to realize signal processing including input signal loading, weight distribution, time delay, and optical power accumulation in optical domain. Due to the high integration of the photonic processing unit, a computing density of 1.04 TOPS/mm<sup>2</sup> was achieved based on this system.

In addition to the Si platform, the TFLN platform can also achieve efficient on-chip optical computing and signal processing [244]. Similarly, on-chip DFB lasers can also be applied as the integrated light sources to improve energy efficiency and system footprint. In 2024, Z. Lin et al. presented an integrated photonic tensor core based on the TFLN platform, combining a III-V laser chip and a charge-integration photoreceiver, shown in Fig. 7(d) [245]. The system can conduct a neural network with a computational speed of 120 GOPS and support fast training with a weight update rate up to 60 GHz, which can perform large-scale matrix-vector multiplications at high speeds.

However, the light sources in the above integration work are all based on an individual III-V DFB chip, which is still a separate one from the on-chip optical computing system (integrated through co-packaging) Although the approach has improved in energy consumption and system size compared to traditional bench-top lasers, there is still much space for optimization in terms of heterogeneous integration on a single chip. Recently, with the development of heterogeneous Si

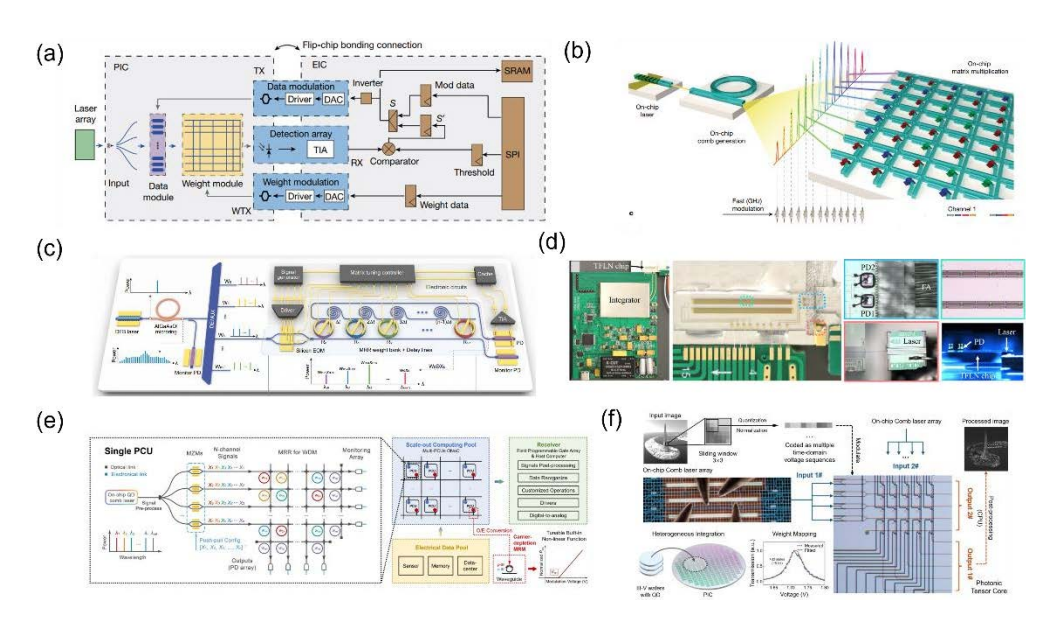


**Fig. 7.** Optical neural networks with integrated lasers. (a) System architecture of a highly integrated 64×64 photonic computing engine. The system has a high speed of 1 GHz frequency and a low latency of 3 ns per cycle, powered by 4-channel DFB laser modules. Reprinted from Ref. [238]. (b) Conceptual illustration of a fully integrated microcombdriven optical neural networks. An on-chip laser can pump an integrated resonator directly to generate a broadband frequency comb. Reprinted from Ref. [242]. (c) An microcomb-based optical convolution accelerator. The resonator is pumped by an integrated DFB laser chip to generate the microcomb. Reprinted from Ref. [243]. (d) Packaged module of an integrated photonic tensor core based on the TFLN platform. A III-V laser chip and a charge-integration photoreceiver are combined with the TFLN chip. Reprinted from Ref. [245]. (e) Architecture of a high-speed optical neural network based on Si heterogeneous integration platforms. The on-chip QD lasers can be used as the light source for computing system. Reprinted from Ref. [246]. (f) The photonic computing unit including on-chip QD comb lasers and MRR array in the Si heterogeneous platform. The fabrication and working flow are shown. Reprinted from Ref. [247].

integration platforms for QD lasers, highly integrated optical neural network systems with lasers on one same chip are emerging. In 2024, Z. Zhou et al. demonstrated a high-speed optical neural network architecture based on heterogeneously integrated QD lasers in Fig. 7(e) [246]. In this fully integrated work, the system has a theoretical computational density of 3.5 TOPS/mm², while maintaining an energy overhead below 29.97 fJ/OP. Based on the optimized software-hardware co-designed strategy, the proposed weight-reuse model obtains 91.128% accuracy on MNIST. Furthermore, they comprehensively optimized all the devices for the parallel photonic computing unit including on-chip lasers and MRR array in Si heterogeneous platform, shown in Fig. 7(f) [247]. This prototype illustrates the potential of Si heterogeneous QD platforms for optical computing, which can reduce the overall system size and manufacturing cost by heterogeneously integrating lasers and signal processing units together on a single chip.

Optical neural networks that use photonic technology for signal processing provide a promising solution for breaking through the performance bottleneck of traditional electronic computing for next-generation AI hardware. However, how to improve the integration scale and density is still a key issue for the deployment of optical computing. By using integrated III-V laser chips, or further, fabricating on-chip lasers and computing systems on a single substrate through

heterogeneous integration, the system integration density and energy efficiency will be greatly optimized, which is conducive to the realization of complex optical neural network functions in the future.

### 4.3. On-chip LiDAR systems

With the continuous advancement of AI technology, autonomous driving has made rapid progress in recent years [248]. In terms of decision-making and system control, AI provides a key foundation for autonomous driving. At the same time, the realization of autonomous driving requires sufficient system perception for sensing and imaging [249], such as speed detection and distance resolution abilities. Under this requirement, LiDAR technology has attracted widespread attention due to the long-distance perception and anti-interference ability. Compared to discrete device solutions, the LiDAR systems on a compact photonic chip has the advantages of high density, large scale, low power consumption and low cost [250–252]. Based on the integrated photonics chip platform [253], LiDAR can be further miniaturized and widely deployed, which will provide AI systems with improved all-round perception capabilities. As the light source, the laser is the core component of on-chip LiDAR systems and will have a direct impact on the cost and size of the system [254]. If the components in the architecture, including the laser, can be integrated on chip scale, the mass-produced wafer-scale LiDARs can be applied to a wider market [255,256].

Due to the advantages of low cost, high stability, industry maturity and high electrical scalability, Si photonics is still the main platform for integrated LiDAR systems [257–261]. In 2009, K. Acoleyen et al. demonstrated off-chip beam steering with a one-dimensional optical phased array (OPA) on Si photonics platform for the first time [262]. In 2013, J. Sun et al. realized a large-scale two-dimensional OPA, where  $64 \times 64$  optical nanoantennas are fabricated in a compact area of 576  $\mu$ m  $\times$  576  $\mu$ m on a Si photonic chip [263]. Furthermore, they reported an  $8 \times 8$  OPA, in which 64 nanoantennas was tailored as Gaussian-shaped distributions [264]. However, most LiDAR systems based on photonic chips still adopt traditional off-chip bench-top lasers, which will constrain the entire system size. The integrated DFB laser chip provides a solution to replace the bench-top lasers for packaging systems. In 2018, A. Martin et al. demonstrated an integrated FMCW LiDAR on a Si platform, where DFB laser is adopted as the light source, and the system can achieve a ranging detection of 60 m with below 5 mW output power [265]. Combined with integrated optical frequency comb technology, the DFB laser can be used as the direct chip-scale pump for the microresonator to generate multi-wavelength signals. In 2023, R. Chen et al. proposed a novel parallel LiDAR solution based on the chaotic microcomb with a wide spectrum range to break through the temporal and frequency congestion, shown in Fig. 8(a) [266]. The nonlinear AlGaAs microresonator is pumped by an integrated III-V DFB laser, and a high chaotic spectrum beyond 12 GHz is demonstrated. The chaotic LiDAR system, which is immune to interference, can achieve a ranging precision of 2 mm and accurate velocity detection for slow movements below 5 mm/s, while a high-resolution 3D image is also illustrated by using 51 comb lines.

For the higher integration level, the laser device needs to be heterogeneously integrated with the OPA system on one single Si chip. Based on the heterogeneous III-V/Si platform, in 2015, J. Huleme et al. demonstrated an integrated free-space beam steering system, which consists of 164 optical components including on-chip lasers [267]. The steering over  $23^{\circ} \times 3.6^{\circ}$  was achieved with  $1^{\circ} \times 0.6^{\circ}$  beam widths, and 138 resolvable spots in the far field were shown. In 2019, W. Xie et al. presented a fully integrated interferometric optical gyroscopes with an area of 4.5 mm<sup>2</sup> and a dense OPA using heterogeneous phase shifters with 4 µm pitch which has low static power consumption below 3 nW, and high speed beyond 1 GHz [268]. Furthermore, in 2022, K. Sayyah et al. demonstrated two fully-integrated frequency-modulated continuous-wave (FMCW) LiDAR systems including the integrated lasers on single Si chips, as illustrated in Fig. 8(b) [269].

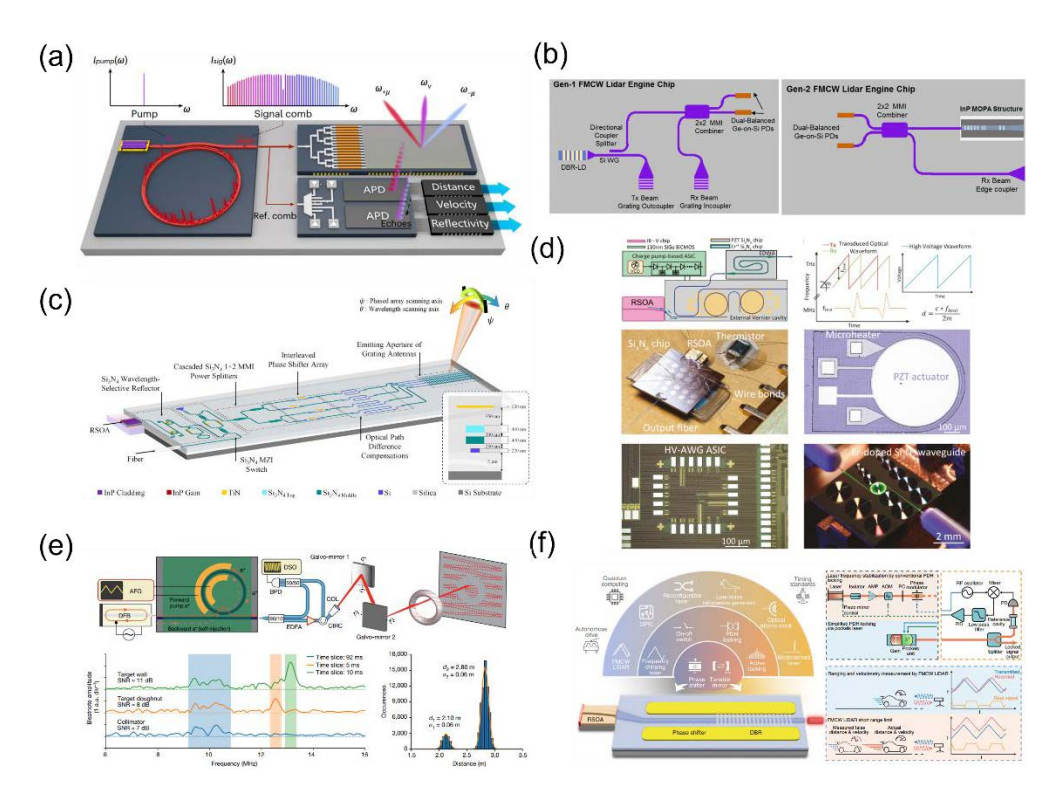


**Fig. 8.** On-chip LiDAR systems with integrated lasers. (a) System architecture of the parallel LiDAR solution based on the chaotic microcomb. The AlGaAs microresonator is pumped by an integrated III-V DFB laser to generate a high chaotic spectrum. Reprinted from Ref. [266]. (b) Schematic of the FMCW LiDAR chip with a heterogeneously integrated laser. Two fully integrated system architectures including the on-chip laser are shown. Reprinted from Ref. [269]. (c) System architecture of the fully integrated LiDAR transmitter. A hybrid tunable external cavity laser and a high-resolution two-dimensional OPA are integrated on the SiN platform. Reprinted from Ref. [272]. (d) Schematic of the photonic-electric integrated LiDAR system. The wafer-scale fabrication process is adopted including III-V semiconductors, SiN photonics, and GeSi bipolar CMOS technology. Reprinted from Ref. [273]. (e) Experiment of the integrated LiDAR system based on the heterogeneous integrated ultrafast tunable laser. The FMCW system based on the laser can achieve a high resolution without signal pre-distortion and active feedback. Reprinted from Ref. [274]. (f) Schematic of integrated Pockels laser on TFLN for LiDAR applications. The device structure and experimental systems are shown. Reprinted from Ref. [275].

Based on the heterogeneous on-chip DBR laser schemes, a maximum detection range of 28 m is achieved, and a detection range of 75 m can be achieved with the adoption of an InP-based integrated optical amplifier.

For the low-loss SiN platform, LiDAR systems can also be fabricated based on SiN to provide more optical power [270,271]. Representatively, in 2023, W. Xu et al. demonstrated a fully integrated LiDAR transmitter including a hybrid integrated widely tunable external cavity laser and a high-resolution two-dimensional OPA on the multi-layer SiN platform in Fig. 8(c) [272]. Two-dimensional beam steering is achieved in a  $140^{\circ} \times 16^{\circ}$  filed with a beam divergence of  $0.051^{\circ} \times 0.016^{\circ}$ . In 2024, A. Lukashchuk et al. presented a photonic-electric integrated LiDAR system in Fig. 8(d), which is based on a wafer-scale process including III-V semiconductors, SiN photonics, and GeSi bipolar CMOS technology [273]. The system consists of a microelectronic

high-voltage arbitrary waveform generator, a hybrid tunable Vernier laser, and an erbium-doped waveguide amplifier, achieving ranging detection at a 10 m distance with a precision level of 10 cm and an acquisition rate of 50 kHz.

Meanwhile, the TFLN platform, with the favorable EO performance, is the emerging platform for optoelectronic systems, and developing heterogeneous lasers on TFLN is the key step to fully integration with multiple functions. For LiDAR applications, in 2023, V. Snigirev et al. demonstrated a tunable laser on a low-loss heterogeneous SiN/LN platform with an ultrafast frequency tuning of 12 PHz/s and the narrow-linewidth lasing can be also achieved by self-injection locking to the laser diode [274]. The FMCW optical ranging based on the integrated laser, as illustrated in Fig. 8(e), can achieve a resolution of 15 cm without signal pre-distortion and active feedback. Recently, in 2025, S. Xue et al. demonstrated a Pockels laser based on the TFLN platform with a narrow intrinsic linewidth of 167 Hz, an optical power of 13 mW and a broad mode-hop-free tuning range of 24 GHz [275]. The device structure and experimental systems are shown in Fig. 8(f). Moreover, a frequency chirping rate of 20 EHz/s and a modulation bandwidth beyond 10 GHz can be provided by the device. Based on the integrated on-chip laser, an FMCW LiDAR system can be constructed with the velocimetry at 40 m/s in 0.4 m and a ranging resolution below 2 cm.

LiDAR technology is an essential perception method for AI systems represented by autonomous driving. With the rapid development and deployment of AI, the system's requirements for sensing capabilities are increasing, which provides the driving force for the evolution of LiDAR technology. The integration of lasers provides a prerequisite guarantee for the on-chip miniaturization of the entire LiDAR system. At present, most studies on on-chip LiDAR systems are still driven by separate laser chips, which can already effectively reduce the overall system size and energy consumption. Moreover, with the development of heterogeneous integration processes on various platforms, the performance of heterogeneous integrated lasers is constantly improving, and the large-scale signal processing system can also be built on the heterogeneous platform, which provides a key foundation for realizing a complete LiDAR system on a single chip.

#### 5. Conclusions

In conclusion, we have reviewed integrated laser technologies for emerging AI applications from device performance to system applications. Beginning with the transmitter research, which is still the primary driving force for the development of integrated lasers, we summarized the technologies, trends, and requirements of the transmitters including integrated pure Si modulators and integrated heterogeneous modulators. Then, we discussed integrated III-V lasers based on different photonic platforms including Si, SiN and TFLN in detail, where the mainstream integration methods including hybrid and heterogeneous integration are both analyzed. For the system application level, we summarized the progress of representative applications for AI including optical interconnections, optical neural networks and on-chip LiDAR systems based on integrated lasers. Integrated lasers are core functional active devices in information photonic systems, and the performance and integration level of lasers will have a direct impact on the overall system functions. Especially in the AI era, various emerging applications have increasingly higher requirements for bandwidth, energy consumption, and cost. While integrated photonic platforms provide a promising solution to satisfy growing demands of AI, the development of high-performance low-cost integrated lasers is the prerequisite for realizing fully integrated photonic systems that can be deployed on a large scale. With the continuous efforts of academia and industry, on-chip integrated lasers hold promise for further significant progress and introduce new vitality into the development of integrated photonics driven by AI.

Funding. Semiconductor Research Corporation (2023-JU-3132).

**Disclosures.** J.E.B. is a co-founder of Nexus Photonics and Quintessent.

Data availability. No data were generated in the presented research.

#### References

- S. Sarkar, "The role of information and communication technology (ICT) in higher education for the 21st century," Science 1, 30–41 (2012).
- R. Heeks, "Do information and communication technologies (ICTs) contribute to development?" J. of Intl. Development 22(5), 625–640 (2010).
- D. R.-J. G.-J. Rydning, J. Reinsel, and J. Gantz, The digitization of the world from edge to core (International Data Corporation: Framingham, 2018) 16, 1–28.
- 4. A. Mehonic and A. J. Kenyon, "Brain-inspired computing needs a master plan," Nature 604(7905), 255–260 (2022).
- 5. I. Augenstein, T. Baldwin, M. Cha, *et al.*, "Factuality challenges in the era of large language models and opportunities for fact-checking," Nat. Mach. Intell. **6**(8), 852–863 (2024).
- T. Wu, S. He, J. Liu, et al., "A brief overview of ChatGPT: The history, status quo and potential future development," IEEE/CAA J. Autom. Sinica 10(5), 1122–1136 (2023).
- A. Casheekar, A. Lahiri, K. Rath, et al., "A contemporary review on chatbots, AI-powered virtual conversational agents, ChatGPT: Applications, open challenges and future research directions," Computer Science Review 52, 100632 (2024).
- R. W. Tkach, "Scaling optical communications for the next decade and beyond," Bell Labs Tech. J. 14(4), 3–9 (2010).
- Q. Cheng, M. Bahadori, M. Glick, et al., "Recent advances in optical technologies for data centers: a review," Optica 5(11), 1354 (2018).
- 10. Y. Hao, S. Xiang, G. Han, *et al.*, "Recent progress of integrated circuits and optoelectronic chips," Sci. China Inf. Sci. **64**(10), 201401 (2021).
- Z. Zhou, R. Chen, X. Li, et al., "Development trends in silicon photonics for data centers," Opt. Fiber Technol. 44, 13–23 (2018).
- N. Li, G. Chen, D. K. Ng, et al., "Integrated lasers on silicon at communication wavelength: a progress review," Adv. Opt. Mater. 10(23), 2201008 (2022).
- F. S. Ujager, S. Zaidi, and U. Younis, "A review of semiconductor lasers for optical communications," in 7th International Symposium on High-capacity Optical Networks and Enabling Technologies, (IEEE, 2010), 107–111.
- 14. N. H. Zhu, Z. Shi, Z. K. Zhang, *et al.*, "Directly modulated semiconductor lasers," IEEE J. Sel. Top. Quantum Electron. **23**(4), 1–5 (2017).
- R. Schwertberger, D. Gold, J. Reithmaier, et al., "Long-wavelength InP-based quantum-dash lasers," IEEE Photonics Technol. Lett. 14(6), 735–737 (2002).
- D. Saxena, S. Mokkapati, P. Parkinson, et al., "Optically pumped room-temperature GaAs nanowire lasers," Nat. Photonics 7(12), 963–968 (2013).
- Y. Zhang, Y. Xu, J. Shi, et al., "Monolithic integrated linear frequency modulated dual-wavelength DFB laser chip with high linearity and its application in long distance ranging," ACS Photonics 10(7), 2344–2352 (2023).
- 18. S. Jia, M.-C. Lo, L. Zhang, *et al.*, "Integrated dual-laser photonic chip for high-purity carrier generation enabling ultrafast terahertz wireless communications," Nat. Commun. **13**(1), 1388 (2022).
- 19. R. Nagarajan, M. Kato, J. Pleumeekers, *et al.*, "InP photonic integrated circuits," IEEE J. Sel. Top. Quantum Electron. **16**(5), 1113–1125 (2010).
- 20. S. Arafin and L. A. Coldren, "Advanced InP photonic integrated circuits for communication and sensing," IEEE J. Sel. Top. Quantum Electron. 24(1), 1–12 (2018).
- M. Smit, K. Williams, and J. Van Der Tol, "Past, present, and future of InP-based photonic integration," APL Photonics 4(5), 050901 (2019).
- Y. Wang, Y. Jiao, and K. Williams, "Scaling photonic integrated circuits with InP technology: A perspective," APL Photonics 9(5), 0200861 (2024).
- L. M. Augustin, R. Santos, E. D. Haan, et al., "InP-based generic foundry platform for photonic integrated circuits," IEEE J. Sel. Top. Quantum Electron. 24(1), 1–10 (2018).
- C. Mukherjee, M. Deng, V. Nodjiadjim, et al., "Towards monolithic indium phosphide (InP)-based electronic photonic technologies for beyond 5G communication systems," Appl. Sci. 11(5), 2393 (2021).
- 25. D. Liang and J. E. Bowers, "Recent progress in lasers on silicon," Nat. Photonics 4(8), 511–517 (2010).
- 26. D. Liang, G. Roelkens, R. Baets, *et al.*, "Hybrid integrated platforms for silicon photonics," Materials 3(3), 1782–1802 (2010).
- 27. Z. Wang, A. Abbasi, U. Dave, *et al.*, "Novel light source integration approaches for silicon photonics," Laser Photonics Rev. **11**(4), 1700063 (2017).
- 28. A. H. Atabaki, S. Moazeni, F. Pavanello, *et al.*, "Integrating photonics with silicon nanoelectronics for the next generation of systems on a chip," Nature **556**(7701), 349–354 (2018).
- S. Y. Siew, B. Li, F. Gao, et al., "Review of silicon photonics technology and platform development," J. Lightwave Technol. 39(13), 4374

  –4389 (2021).
- S. Shekhar, W. Bogaerts, L. Chrostowski, et al., "Roadmapping the next generation of silicon photonics," Nat. Commun. 15(1), 751 (2024).

- 31. Y. Su, Y. Zhang, C. Qiu, *et al.*, "Silicon photonic platform for passive waveguide devices: materials, fabrication, and applications," Adv. Materials Technologies **5**(8), 1901153 (2020).
- 32. P. Dong, Y.-K. Chen, G.-H. Duan, *et al.*, "Silicon photonic devices and integrated circuits," Nanophotonics **3**(4-5), 215–228 (2014).
- 33. L. Sun, Y. Zhang, Y. He, *et al.*, "Subwavelength structured silicon waveguides and photonic devices," Nanophotonics **9**(6), 1321–1340 (2020).
- 34. G. T. Reed, G. Mashanovich, F. Y. Gardes, et al., "Silicon optical modulators," Nat. Photonics 4(8), 518-526 (2010).
- G. T. Reed, G. Z. Mashanovich, F. Y. Gardes, et al., "Recent breakthroughs in carrier depletion based silicon optical modulators," Nanophotonics 3(4-5), 229–245 (2014).
- 36. A. Rahim, A. Hermans, B. Wohlfeil, *et al.*, "Taking silicon photonics modulators to a higher performance level: state-of-the-art and a review of new technologies," Adv. Photonics **3**(02), 024003 (2021).
- 37. X. Zhou, D. Yi, D. W. U. Chan, *et al.*, "Silicon photonics for high-speed communications and photonic signal processing," npj Nanophotonics **1**(1), 27 (2024).
- 38. J. Mulcahy, F. H. Peters, and X. Dai, "Modulators in silicon photonics—heterogenous integration & and beyond," in *Photonics*, (MDPI, 2022), 40.
- 39. M. Casalino, G. Coppola, R. M. De La Rue, *et al.*, "State-of-the-art all-silicon sub-bandgap photodetectors at telecom and datacom wavelengths," Laser & Photonics Reviews **10**(6), 895–921 (2016).
- Z. Xiao, W. Liu, S. Xu, et al., "Recent progress in silicon-based photonic integrated circuits and emerging applications," Advanced Optical Materials 11(20), 2301028 (2023).
- G. Chen, Y. Yu, Y. Shi, et al., "High-speed photodetectors on silicon photonics platform for optical interconnect," Laser & Photonics Reviews 16(12), 2200117 (2022).
- 42. X. Wang and J. Liu, "Emerging technologies in Si active photonics," J. Semicond. 39(6), 061001 (2018).
- 43. J. Michel, J. Liu, and L. C. Kimerling, "High-performance Ge-on-Si photodetectors," Nat. Photonics 4(8), 527–534 (2010).
- F. Priolo, T. Gregorkiewicz, M. Galli, et al., "Silicon nanostructures for photonics and photovoltaics," Nature Nanotech. 9(1), 19–32 (2014).
- L.-D. Yuan, H.-X. Deng, S.-S. Li, et al., "Unified theory of direct or indirect band-gap nature of conventional semiconductors," Phys. Rev. B 98(24), 245203 (2018).
- L. Pavesi, "Silicon-based light sources for silicon integrated circuits," Advances in Optical Technologies 2008(1), 416926 (2008).
- C. Xiang, S. M. Bowers, A. Bjorlin, et al., "Perspective on the future of silicon photonics and electronics," Appl. Phys. Lett. 118(22), 220501 (2021).
- 48. Z. Zhou, B. Yin, and J. Michel, "On-chip light sources for silicon photonics," Light: Sci. Appl. 4(11), e358 (2015).
- 49. M. Tang, J.-S. Park, Z. Wang, *et al.*, "Integration of III-V lasers on Si for Si photonics," Progress in Quantum Electronics **66**, 1–18 (2019).
- D. Liang and J. E. Bowers, "Recent progress in heterogeneous III-V-on-silicon photonic integration," Light: Advanced Manufacturing 2(1), 59–83 (2021).
- 51. Z. Zhou, X. Ou, Y. Fang, et al., "Prospects and applications of on-chip lasers," eLight 3(1), 1 (2023).
- 52. Y. Han, H. Park, J. Bowers, *et al.*, "Recent advances in light sources on silicon," Adv. Opt. Photonics **14**(3), 404 (2022).
- C. Xiang, W. Jin, and J. E. Bowers, "Silicon nitride passive and active photonic integrated circuits: trends and prospects," Photonics Res. 10(6), A82–A96 (2022).
- 54. Q. Luo, F. Bo, Y. Kong, *et al.*, "Advances in lithium niobate thin-film lasers and amplifiers: a review," Adv. Photonics **5**(03), 034002 (2023).
- 55. S. Fathpour, "Emerging heterogeneous integrated photonic platforms on silicon," Nanophotonics 4(1), 143–164 (2015).
- 56. C. Xiang, W. Jin, D. Huang, *et al.*, "High-performance silicon photonics using heterogeneous integration," IEEE J. Select. Topics Quantum Electron. **28**(3), 1–15 (2022).
- H. Wang, H. Chai, Z. Lv, et al., "Silicon photonic transceivers for application in data centers," J. Semicond. 41(10), 101301 (2020).
- 58. A. Liu, R. Jones, L. Liao, *et al.*, "A high-speed silicon optical modulator based on a metal-oxide-semiconductor capacitor," Nature **427**(6975), 615–618 (2004).
- D. Patel, S. Ghosh, M. Chagnon, et al., "Design, analysis, and transmission system performance of a 41 GHz silicon photonic modulator," Opt. Express 23(11), 14263–14287 (2015).
- H. Xu, X. Xiao, X. Li, et al., "High speed silicon Mach-Zehnder modulator based on interleaved PN junctions," Opt. Express 20(14), 15093–15099 (2012).
- 61. M. Li, L. Wang, X. Li, *et al.*, "Silicon intensity Mach–Zehnder modulator for single lane 100 Gb/s applications," Photonics Res. **6**(2), 109 (2018).
- 62. H. Zhang, M. Li, Y. Zhang, *et al.*, "800 Gbit/s transmission over 1 km single-mode fiber using a four-channel silicon photonic transmitter," Photonics Res. **8**(11), 1776 (2020).
- K. Li, D. J. Thomson, S. Liu, et al., "An integrated CMOS-silicon photonics transmitter with a 112 gigabaud transmission and picojoule per bit energy efficiency," Nat. Electron. 6(11), 910–921 (2023).

- 64. A. D. Simard, B. Filion, D. Patel, *et al.*, "Segmented silicon MZM for PAM-8 transmissions at 114 Gb/s with binary signaling," Opt. Express **24**(17), 19467–19472 (2016).
- A. Mohammadi, Z. Zheng, X. Zhang, et al., "Segmented silicon modulator with a bandwidth beyond 67 GHz for high-speed signaling," J. Lightwave Technol. 41(15), 5059–5066 (2023).
- Z. Yao, K. Wu, B. X. Tan, et al., "Integrated silicon photonic microresonators: emerging technologies," IEEE J. Select. Topics Quantum Electron. 24(1), 1–11 (2018).
- Q. Xu, B. Schmidt, S. Pradhan, et al., "Micrometre-scale silicon electro-optic modulator," Nature 435(7040), 325–327 (2005).
- 68. W. Bogaerts, P. De Heyn, T. Van Vaerenbergh, *et al.*, "Silicon microring resonators," Laser & Photonics Reviews **6**(1), 47–73 (2012).
- 69. J. Sun, R. Kumar, M. Sakib, *et al.*, "A 128 Gb/s PAM4 silicon microring modulator with integrated thermo-optic resonance tuning," J. Lightwave Technol. **37**(1), 110–115 (2019).
- D. W. U. Chan, X. Wu, Z. Zhang, et al., "C-band 67 GHz silicon photonic microring modulator for dispersion-uncompensated 100 Gbaud PAM-4," Opt. Lett. 47(11), 2935–2938 (2022).
- D. W. U. Chan, X. Wu, C. Lu, et al., "Efficient 330-Gb/s PAM-8 modulation using silicon microring modulators," Opt. Lett. 48(4), 1036–1039 (2023).
- 72. Y. Yuan, Y. Peng, W. V. Sorin, *et al.*, "A 5 × 200 Gbps microring modulator silicon chip empowered by two-segment Z-shape junctions," Nat. Commun. **15**(1), 918 (2024).
- 73. R. Soref and B. Bennett, "Electrooptical effects in silicon," IEEE J. Quantum Electron. 23(1), 123–129 (1987).
- C. Han, Z. Zheng, H. Shu, et al., "Slow-light silicon modulator with 110-GHz bandwidth," Sci. Adv. 9(42), eadi5339 (2023).
- 75. C. Han, Q. Yang, J. Qin, et al., "Exploring 400 Gbps/lambda and beyond with AI-accelerated silicon photonic slow-light technology," Nat. Commun. 16(1), 6547 (2025).
- D. Zhu, L. Shao, M. Yu, et al., "Integrated photonics on thin-film lithium niobate," Adv. Opt. Photonics 13(2), 242 (2021).
- M. Zhang, C. Wang, P. Kharel, et al., "Integrated lithium niobate electro-optic modulators: when performance meets scalability," Optica 8(5), 652 (2021).
- L. Alloatti, R. Palmer, S. Diebold, et al., "100 GHz silicon-organic hybrid modulator," Light: Sci. Appl. 3(5), e173 (2014).
- G. W. Lu, J. Hong, F. Qiu, et al., "High-temperature-resistant silicon-polymer hybrid modulator operating at up to 200 Gbit s(-1) for energy-efficient datacentres and harsh-environment applications," Nat. Commun. 11(1), 4224 (2020).
- J. Liu, M. Beals, A. Pomerene, et al., "Waveguide-integrated, ultralow-energy GeSi electro-absorption modulators," Nat. Photonics 2(7), 433–437 (2008).
- 81. X. Hu, D. Wu, D. Chen, *et al.*, "280 Gbit/s PAM-4 Ge/Si electro-absorption modulator with 3-dB bandwidth beyond 110 GHz," in *Optical Fiber Communication Conference*, (Optica Publishing Group, 2023), Th4A. 3.
- 82. M. Baier, N. Grote, M. Moehrle, et al., "Integrated transmitter devices on InP exploiting electro-absorption modulation," PhotoniX 1(1), 4 (2020).
- 83. A. Boes, L. Chang, C. Langrock, *et al.*, "Lithium niobate photonics: Unlocking the electromagnetic spectrum," Science **379**(6627), eabj4396 (2023).
- H. Han, S. Ruan, and B. Xiang, "Heterogeneously integrated photonics based on thin film lithium niobate platform," Laser & Photonics Reviews 19(1), 2400649 (2025).
- 85. Y. Hu, D. Zhu, S. Lu, *et al.*, "Integrated electro-optics on thin-film lithium niobate," Nature Reviews Physics **7**(5), 237–254 (2025).
- C. Wang, M. Zhang, X. Chen, et al., "Integrated lithium niobate electro-optic modulators operating at CMOS-compatible voltages," Nature 562(7725), 101–104 (2018).
- 87. M. He, M. Xu, Y. Ren, *et al.*, "High-performance hybrid silicon and lithium niobate Mach–Zehnder modulators for 100 Gbit s–1 and beyond," Nat. Photonics **13**(5), 359–364 (2019).
- 88. P. O. Weigel, J. Zhao, K. Fang, *et al.*, "Bonded thin film lithium niobate modulator on a silicon photonics platform exceeding 100 GHz 3-dB electrical modulation bandwidth," Opt. Express **26**(18), 23728–23739 (2018).
- 89. B.-C. Pan, H.-X. Liu, H.-C. Xu, *et al.*, "Ultra-compact lithium niobate microcavity electro-optic modulator beyond 110 GHz," Chip **1**(4), 100029 (2022).
- F. Yang, X. Fang, X. Chen, et al., "Monolithic thin film lithium niobate electro-optic modulator with over 110 GHz bandwidth," Chin. Opt. Lett. 20(2), 022502 (2022).
- 91. F. Arab Juneghani, M. Gholipour Vazimali, J. Zhao, *et al.*, "Thin-film lithium niobate optical modulators with an extrapolated bandwidth of 170 GHz," Advanced Photonics Res. **4**(1), 2200216 (2023).
- 92. X. Meng, C. Yuan, X. Cheng, *et al.*, "Thin-film lithium niobate modulators with ultra-high modulation efficiency," Laser & Photonics Reviews **19**(1), 2400809 (2025).
- 93. J. Shen, Y. Zhang, L. Zhang, et al., "Highly efficient slow-light Mach–Zehnder modulator achieving 0.21 V cm efficiency with bandwidth surpassing 110 GHz," Laser & Photonics Reviews 19(8), 2401092 (2025).
- 94. A. Ostrovskis, S. El-Busaidy, T. Salgals, et al., "Optical amplification-free 400 Gbps net bitrate links with a TFLN-based transmitter," in *Optical Fiber Communication Conference*, (Optica Publishing Group, 2025), M1G. 1.

- 95. Y. Yamaguchi, P. Zhu, P. T. Dat, *et al.*, "Fully packaged 100-GHz-bandwidth EO-equalizer-integrated TFLN modulator with record-high slope efficiency enabling 200-GBaud signaling," in *Optical Fiber Communication Conference*, (Optica Publishing Group, 2025), Th4D. 4.
- 96. C. St-Arnault, S. Bernal, D. Kita, *et al.*, "Net 3.2 Tbps 225 Gbaud PAM4 O-Band IM/DD 2 km transmission using FR8 and DR8 with a CMOS 3 nm SerDes and TFLN modulators," *OFC* Th4b.1 (2025).
- 97. E. Berikaa, M. S. Alam, W. Li, *et al.*, "TFLN MZMs and next-Gen DACs: enabling beyond 400 Gbps IMDD O-band and C-band transmission," IEEE Photonics Technology Letters **35**(15), 850–853 (2023).
- C. St-Arnault, S. Bernal, E. Berikaa, et al., "Net 1.6 Tbps (4× 400Gbps/λ) O-Band IM/DD transmission Over 2 km using uncooled DFB lasers on the LAN-WDM grid and Sub-1 V Drive TFLN modulators," in 2024 Optical Fiber Communications Conference and Exhibition (OFC), (IEEE, 2024), 1–3.
- 99. A. N. R. Ahmed, S. Nelan, S. Shi, *et al.*, "Subvolt electro-optical modulator on thin-film lithium niobate and silicon nitride hybrid platform," Opt. Lett. **45**(5), 1112–1115 (2020).
- 100. T. Vanackere, T. Vandekerckhove, L. Bogaert, et al., "Heterogeneous integration of a high-speed lithium niobate modulator on silicon nitride using micro-transfer printing," APL Photonics 8(8), 086102 (2023).
- 101. Z. Ruan, K. Chen, Z. Wang, *et al.*, "High-performance electro-optic modulator on silicon nitride platform with heterogeneous integration of lithium niobate," Laser & Photonics Reviews **17**(4), 2200327 (2023).
- 102. I. Taghavi, M. Moridsadat, A. Tofini, et al., "Polymer modulators in silicon photonics: review and projections," Nanophotonics 11(17), 3855–3871 (2022).
- 103. C. Eschenbaum, A. Mertens, C. Füllner, et al., "Thermally stable silicon-organic hybrid (SOH) Mach-Zehnder modulator for 140 GBd PAM4 transmission with sub-1 V drive signals," in 2022 European Conference on Optical Communication (ECOC), (IEEE, 2022), 1–4.
- 104. H. Yu, B. Li, L. Wang, et al., "Polymer micro-ring modulator on silicon nitride platform," Appl. Phys. Lett. 123(19), 191111 (2023).
- 105. D. W. U. Chan, G. Zhou, X. Wu, et al., "A compact 112-Gbaud PAM-4 silicon photonics transceiver for short-reach interconnects," J. Lightwave Technol. 40(8), 2265–2273 (2022).
- 106. S. Liang, D. Lu, L. Zhao, et al., "Fabrication of InP-based monolithically integrated laser transmitters," Sci. China Inf. Sci. 61(8), 080405 (2018).
- 107. Z. Sun, W. Sun, R. Xiao, et al., "Enhanced performance of wavelength-tunable EML based on REC technique," J. Lightwave Technol. 43(1), 271–279 (2025).
- 108. J. Zhang, J. Yu, and H.-C. Chien, "EML-based IM/DD 400G (4x 112.5-Gbit/s) PAM-4 over 80 km SSMF based on linear pre-equalization and nonlinear LUT pre-distortion for inter-DCI applications," in *Optical Fiber Communication Conference*, (Optica Publishing Group, 2017), W4I. 4.
- 109. W. Li, C. St-Arnault, Z. Wei, et al., "Net 200 Gbps O-band IM/DD transmission over 80 km SMF using InP EML with sub 1-Vpp driving signal and QD-SOA," in ECOC 2024; 50th European Conference on Optical Communication, (VDE, 2024), 55–58.
- 110. H. Asakura, K. Nishimura, S. Yamauchi, *et al.*, "384-Gb/s/lane PAM8 operation using 76-GHz bandwidth EA-DFB laser at 50°C with 1.0-Vpp Swing over 2-km transmission," in *Optical Fiber Communication Conference*, (Optica Publishing Group, 2022), Th4C. 4.
- 111. H. Asakura, K. Nishimura, S. Yamauchi, et al., "420 Gbps PAM8 operation using 93 GHz bandwidth lumped-electrode type EA-DFB laser at 50° C beyond 400 Gbps/lane," in 2022 European Conference on Optical Communication (ECOC), (IEEE, 2022), 1–3.
- 112. H. Asakura, "400 Gbps semi-cooled lumped-electrode EA-DFB laser operating at 200 Gbaud PAM4 modulation with 0.6 Vpp," in *Proceeding 2024 European Conference on Optical Communication (ECOC)*, (2024), Th3A. 1.
- 113. X. Chen, P. Liao, F. Tang, et al., "540Gbps IMDD transmission over 30 km SMF using 110 GHz bandwidth InP EML," in *Optical Fiber Communication Conference*, (Optica Publishing Group, 2025), Th4B. 2.
- 114. J.-H. Han, F. Boeuf, J. Fujikata, et al., "Efficient low-loss InGaAsP/Si hybrid MOS optical modulator," Nat. Photonics 11(8), 486–490 (2017).
- 115. T. Hiraki, T. Aihara, K. Hasebe, et al., "Heterogeneously integrated III–V/Si MOS capacitor Mach–Zehnder modulator," Nat. Photonics 11(8), 482–485 (2017).
- 116. H. Tang, Q. Li, C. P. Ho, et al., "Modulation bandwidth improvement of III-V/Si hybrid MOS optical modulator by reducing parasitic capacitance," Opt. Express 30(13), 22848–22859 (2022).
- 117. R. Koscica, P. Pintus, M. A. Tran, et al., "63 fJ/bit heterogeneous III-V on Si modulator for the C band," in 2022 Optical Fiber Communications Conference and Exhibition (OFC), (IEEE, 2022), 1–3.
- 118. P. Pintus, A. Singh, W. Xie, *et al.*, "Ultralow voltage, high-speed, and energy-efficient cryogenic electro-optic modulator," Optica **9**(10), 1176 (2022).
- P. J. Winzer and D. T. Neilson, "From scaling disparities to integrated parallelism: A decathlon for a decade," J. Lightwave Technol. 35(5), 1099–1115 (2017).
- 120. E. Agrell, M. Karlsson, F. Poletti, et al., "Roadmap on optical communications," J. Opt. 26(9), 093001 (2024).
- 121. X. Zhou, R. Urata, and H. Liu, "Beyond 1 Tb/s intra-data center interconnect technology: IM-DD OR coherent?" J. Lightwave Technol. 38(2), 475–484 (2020).
- 122. G. Rizzelli, P. Torres-Ferrera, F. Forghieri, *et al.*, "An analytical model for performance estimation in modern high-capacity IMDD systems," J. Lightwave Technol. **42**(5), 1443–1452 (2024).

- 123. X. Pang, O. Ozolins, R. Lin, *et al.*, "200 Gbps/lane IM/DD technologies for short reach optical interconnects," J. Lightwave Technol. **38**(2), 492–503 (2020).
- 124. Q. Zhao, Z. Zhang, B. Wu, *et al.*, "Noise-sidebands-free and ultra-low-RIN 1.5 μm single-frequency fiber laser towards coherent optical detection," Photonics Res. **6**(4), 326–331 (2018).
- 125. X. She, B. Xiong, C. Sun, et al., "Coherently combined DFB laser array chip with reduced relative intensity noise," IEEE Photonics Technol. Lett. 33(18), 986–989 (2021).
- 126. Y. Shi, Y. Zhang, Y. Wan, et al., "Silicon photonics for high-capacity data communications," Photonics Res. 10(9), A106–A134 (2022).
- 127. A. Netherton, M. Dumont, Z. Nelson, et al., "High capacity, low power, short reach integrated silicon photonic interconnects," Photonics Res. 12(11), A69 (2024).
- 128. H. Shu, L. Chang, Y. Tao, et al., "Microcomb-driven silicon photonic systems," Nature 605(7910), 457-463 (2022).
- 129. C. Doerr and L. Chen, "Silicon photonics in optical coherent systems," Proc. IEEE 106(12), 2291-2301 (2018).
- 130. S. Bernal, M. Dumont, E. Berikaa, et al., "12.1 terabit/second data center interconnects using O-band coherent transmission with QD-MLL frequency combs," Nat. Commun. 15(1), 7741 (2024).
- 131. X. Zhang, Z. Zhou, Y. Guo, *et al.*, "High-coherence parallelization in integrated photonics," Nat. Commun. **15**(1), 7892 (2024).
- B. Corcoran, A. Mitchell, R. Morandotti, et al., "Optical microcombs for ultrahigh-bandwidth communications," Nat. Photonics 19(5), 451–462 (2025).
- 133. Y. Li, Y. Zhang, L. Zhang, *et al.*, "Silicon and hybrid silicon photonic devices for intra-datacenter applications: state of the art and perspectives," Photonics Res. **3**(5), B10–B27 (2015).
- 134. P. Dong, "Silicon photonic integrated circuits for wavelength-division multiplexing applications," IEEE J. Select. Topics Quantum Electron. 22(6), 370–378 (2016).
- 135. J. B. Driscoll, P. Doussiere, S. Islam, et al., "First 400G 8-channel CWDM silicon photonic integrated transmitter," in 2018 IEEE 15th International Conference on Group IV Photonics (GFP), (IEEE, 2018), 1–2.
- 136. H. Yu, J. Doylend, W. Lin, et al., "100Gbps CWDM4 silicon photonics transmitter for 5G applications," in *Optical Fiber Communication Conference*, (Optica Publishing Group, 2019), W3E. 4.
- 137. J. C. Norman, D. Jung, Z. Zhang, *et al.*, "A review of high-performance quantum dot lasers on silicon," IEEE J. Quantum Electron. **55**(2), 1–11 (2019).
- 138. L. Carroll, J.-S. Lee, C. Scarcella, *et al.*, "Photonic packaging: transforming silicon photonic integrated circuits into photonic devices," Applied Sciences **6**(12), 426 (2016).
- 139. X. Mu, S. Wu, L. Cheng, et al., "Edge couplers in silicon photonic integrated circuits: A review," Applied Sciences 10(4), 1538 (2020).
- 140. A. Marinins, S. Hänsch, H. Sar, et al., "Wafer-scale hybrid integration of InP DFB lasers on Si photonics by flip-chip bonding with sub-300 nm alignment precision," IEEE J. Select. Topics Quantum Electron. 29, 1–11 (2022).
- 141. Y. Tao, H. Shu, X. Wang, et al., "Hybrid-integrated high-performance microwave photonic filter with switchable response," Photonics Res. 9(8), 1569–1580 (2021).
- 142. Y. Tao, F. Yang, Z. Tao, *et al.*, "Fully on-chip microwave photonic instantaneous frequency measurement system," Laser & Photonics Reviews **16**(11), 2200158 (2022).
- 143. M. R. Billah, M. Blaicher, T. Hoose, *et al.*, "Hybrid integration of silicon photonics circuits and InP lasers by photonic wire bonding," Optica **5**(7), 876–883 (2018).
- 144. A. W. Fang, H. Park, O. Cohen, et al., "Electrically pumped hybrid AlGaInAs-silicon evanescent laser," Opt. Express 14(20), 9203–9210 (2006).
- 145. A. W. Fang, E. Lively, Y.-H. Kuo, et al., "A distributed feedback silicon evanescent laser," Opt. Express 16(7), 4413–4419 (2008).
- 146. A. W. Fang, B. R. Koch, R. Jones, et al., "A distributed Bragg reflector silicon evanescent laser," IEEE Photonics Technol. Lett. 20(20), 1667–1669 (2008).
- 147. M. N. Sysak, J. O. Anthes, J. E. Bowers, et al., "Integration of hybrid silicon lasers and electroabsorption modulators," Opt. Express 16(17), 12478–12486 (2008).
- 148. S. Keyvaninia, S. Verstuyft, L. Van Landschoot, et al., "Heterogeneously integrated III-V/silicon distributed feedback lasers," Opt. Lett. 38(24), 5434–5437 (2013).
- 149. H. Shao, S. Keyvaninia, M. Vanwolleghem, *et al.*, "Heterogeneously integrated III–V/silicon dual-mode distributed feedback laser array for terahertz generation," Opt. Lett. **39**(22), 6403–6406 (2014).
- 150. A. Rahim, T. Spuesens, R. Baets, et al., "Open-access silicon photonics: Current status and emerging initiatives," Proc. IEEE 106(12), 2313–2330 (2018).
- 151. G.-H. Duan, S. Olivier, S. Malhouitre, *et al.*, "New advances on heterogeneous integration of III–V on silicon," J. Lightwave Technol. **33**(5), 976–983 (2015).
- 152. R. Won, "Integrating silicon photonics," Nat. Photonics 4(8), 498–499 (2010).
- 153. R. Jones, P. Doussiere, J. B. Driscoll, et al., "Heterogeneously integrated InPvsilicon photonics: fabricating fully functional transceivers," IEEE Nanotechnology Mag. 13(2), 17–26 (2019).
- 154. B. Koch, A. Alduino, L. Liao, et al., "A 4× 12.5 Gb/s CWDM Si photonics link using integrated hybrid silicon lasers," in CLEO: Science and Innovations, (Optica Publishing Group, 2011), CThP5.
- 155. P. D. H. Yu, D. Patel, W. Lin, et al., "400Gbps fully integrated DR4 silicon photonics transmitter for data center applications," Optical Fiber Communication Conference (OFC) T3H.6 (2020).

- 156. H. Yu, D. Patel, W. Liu, et al., "800 Gbps fully integrated silicon photonics transmitter for data center applications," in *Optical Fiber Communication Conference*, (Optica Publishing Group, 2022), M2D. 7.
- 157. T. Hiraki, T. Aihara, Y. Maeda, et al., "Over-67-GHz-bandwidth membrane InGaAlAs electro-absorption modulator integrated with DFB laser on Si platform," J. Lightwave Technol. 41(3), 880–887 (2023).
- 158. E. Norberg, H. Shi, J. Sonkoly, *et al.*, "Silicon photonics platform with heterogeneously integrated lasers and EAMs for 1.6/3.2 T," in *Optical Fiber Communication Conference*, (Optica Publishing Group, 2025), M3K. 3.
- 159. A. Ostrovskis, K. Szczerba, T. Salgals, et al., "Heterogeneously integrated InP electro-absorption modulator for beyond 300 Gb/s optical links," J. Lightwave Technol. 43(4), 1826–1836 (2025).
- 160. Y. De Koninck, C. Caer, D. Yudistira, *et al.*, "GaAs nano-ridge laser diodes fully fabricated in a 300-mm CMOS pilot line," Nature **637**(8044), 63–69 (2025).
- 161. S. Pan, V. Cao, M. Liao, et al., "Recent progress in epitaxial growth of III–V quantum-dot lasers on silicon substrate," J. Semicond. 40(10), 101302 (2019).
- 162. M. Liao, S. Chen, J.-S. Park, et al., "III–V quantum-dot lasers monolithically grown on silicon," Semicond. Sci. Technol. 33(12), 123002 (2018).
- 163. F. Grillot, J. C. Norman, J. Duan, et al., "Physics and applications of quantum dot lasers for silicon photonics," Nanophotonics 9(6), 1271–1286 (2020).
- 164. Y. Wan, S. Zhang, J. C. Norman, et al., "Tunable quantum dot lasers grown directly on silicon," Optica 6(11), 1394 (2019).
- 165. Y. Wan, C. Xiang, J. Guo, *et al.*, "High speed evanescent quantum-dot lasers on Si," Laser & Photonics Reviews **15**(8), 2100057 (2021).
- 166. C. Shang, E. Hughes, Y. Wan, et al., "High-temperature reliable quantum-dot lasers on Si with misfit and threading dislocation filters," Optica 8(5), 749 (2021).
- 167. C. Shang, K. Feng, E. T. Hughes, et al., "Electrically pumped quantum-dot lasers grown on 300 mm patterned Si photonic wafers," Light: Sci. Appl. 11(1), 299 (2022).
- 168. M. Dumont, S. Liu, M. Kennedy, et al., "High-efficiency quantum dot lasers as comb sources for DWDM applications," Applied Sciences 12(4), 1836 (2022).
- 169. B. Dong, M. Dumont, O. Terra, et al., "Broadband quantum-dot frequency-modulated comb laser," Light: Sci. Appl. 12(1), 182 (2023).
- 170. B. Dong, Y. Wan, W. W. Chow, et al., "Turnkey locking of quantum-dot lasers directly grown on Si," Nat. Photonics 18(7), 669–676 (2024).
- 171. A. Liu, M. Davenport, J. Norman, et al., "Multi-wavelength quantum dot comb lasers," OFC W1G.3 (2025).
- 172. D. J. Blumenthal, R. Heideman, D. Geuzebroek, *et al.*, "Silicon nitride in silicon photonics," Proc. IEEE **106**(12), 2209–2231 (2018).
- 173. D. Tan, K. Ooi, and D. Ng, "Nonlinear optics on silicon-rich nitride—a high nonlinear figure of merit CMOS platform," Photonics Res. 6(5), B50–B66 (2018).
- 174. Z. Sun, Y. Li, B. Bai, et al., "Silicon nitride-based Kerr frequency combs and applications in metrology," Adv. Photonics 4(06), 064001 (2022).
- 175. K.-J. Boller, A. van Rees, Y. Fan, *et al.*, "Hybrid integrated semiconductor lasers with silicon nitride feedback circuits," in *Photonics*, (Multidisciplinary Digital Publishing Institute, 2020), 4.
- 176. D. J. Moss, R. Morandotti, A. L. Gaeta, *et al.*, "New CMOS-compatible platforms based on silicon nitride and Hydex for nonlinear optics," Nat. Photonics **7**(8), 597–607 (2013).
- 177. K. A. Buzaverov, A. S. Baburin, E. V. Sergeev, *et al.*, "Silicon nitride integrated photonics from visible to mid-infrared spectra," Laser & Photonics Reviews **18**(12), 2400508 (2024).
- 178. T. Sharma, J. Wang, B. K. Kaushik, *et al.*, "Review of recent progress on silicon nitride-based photonic integrated circuits," IEEE Access **8**, 195436–195446 (2020).
- 179. M. A. Tran, D. Huang, and J. E. Bowers, "Tutorial on narrow linewidth tunable semiconductor lasers using Si/III-V heterogeneous integration," APL Photonics 4(11), 111101 (2019).
- 180. C. Xiang, P. A. Morton, and J. E. Bowers, "Ultra-narrow linewidth laser based on a semiconductor gain chip and extended Si(3)N(4) Bragg grating," Opt. Lett. 44(15), 3825–3828 (2019).
- 181. Y. Fan, A. van Rees, P. J. M. van der Slot, et al., "Hybrid integrated InP-Si(3)N(4) diode laser with a 40-Hz intrinsic linewidth," Opt. Express 28(15), 21713–21728 (2020).
- 182. J. Li, B. Zhang, S. Yang, et al., "Robust hybrid laser linewidth reduction using Si3N4-based subwavelength hole defect assisted microring reflector," Photonics Res. 9(4), 558 (2021).
- 183. A. Siddharth, T. Wunderer, G. Lihachev, et al., "Near ultraviolet photonic integrated lasers based on silicon nitride," APL Photonics 7(4), 046108 (2022).
- 184. S. Cuyvers, B. Haq, C. Op de Beeck, et al., "Low noise heterogeneous III-V-on-Silicon-nitride mode-locked comb laser," Laser & Photonics Reviews 15(8), 2000485 (2021).
- 185. A. Liu, P. Wolf, J. A. Lott, et al., "Vertical-cavity surface-emitting lasers for data communication and sensing," Photonics Res. 7(2), 121 (2019).
- 186. J. Goyvaerts, A. Grabowski, J. Gustavsson, et al., "Enabling VCSEL-on-silicon nitride photonic integrated circuits with micro-transfer-printing," Optica 8(12), 1573 (2021).
- 187. C. Xiang, W. Jin, J. Guo, et al., "Narrow-linewidth III-V/Si/Si3N4 laser using multilayer heterogeneous integration," Optica 7(1), 20 (2020).

- 188. C. Xiang, J. Guo, W. Jin, et al., "High-performance lasers for fully integrated silicon nitride photonics," Nat. Commun. 12(1), 6650 (2021).
- 189. C. Xiang, J. Liu, J. Guo, et al., "Laser soliton microcombs heterogeneously integrated on silicon," Science 373(6550), 99-103 (2021).
- 190. J. Guo, C. A. McLemore, C. Xiang, et al., "Chip-based laser with 1-hertz integrated linewidth," Science advances 8(43), eabp9006 (2022).
- 191. C. Xiang, W. Jin, O. Terra, et al., "3D integration enables ultralow-noise isolator-free lasers in silicon photonics," Nature 620(7972), 78-85 (2023).
- 192. M. Tran, Z. Zhang, B. Shen, et al., "Heterogeneous photonics in visible and beyond," in CLEO: Applications and Technology, (Optica Publishing Group, 2024), AW3J. 3.
- 193. T. Komljenovic, M. Tran, Z. Zhang, et al., "Broadband Heterogeneous Silicon-Nitride Photonics," in 2023 Conference on Lasers and Electro-Optics (CLEO), (IEEE, 2023), 1–2.
- 194. C. Zhang, M. A. Tran, Z. Zhang, et al., "Integrated photonics beyond communications," Appl. Phys. Lett. 123(23),
- 195. X. Lu, L. Chang, M. A. Tran, et al., "Emerging integrated laser technologies in the visible and short near-infrared regimes," Nat. Photonics 18(10), 1010-1023 (2024).
- 196. H. Park, C. Zhang, M. A. Tran, et al., "Heterogeneous silicon nitride photonics," Optica 7(4), 336 (2020).
- 197. M. A. Tran, C. Zhang, T. J. Morin, et al., "Extending the spectrum of fully integrated photonics to submicrometre wavelengths," Nature 610(7930), 54-60 (2022).
- 198. Z. Zhang, B. Shen, M. A. Tran, et al., "Photonic integration platform for rubidium sensors and beyond," Optica 10(6), 752 (2023).
- 199. Y. Han, X. Zhang, F. Huang, et al., "Electrically pumped widely tunable O-band hybrid lithium niobite/III-V laser," Opt. Lett. 46(21), 5413-5416 (2021).
- 200. A. Shams-Ansari, D. Renaud, R. Cheng, et al., "Electrically pumped laser transmitter integrated on thin-film lithium niobate," Optica 9(4), 408 (2022).
- 201. M. Li, L. Chang, L. Wu, et al., "Integrated Pockels laser," Nat. Commun. 13(1), 5344 (2022).
- 202. J. Ling, J. Staffa, H. Wang, et al., "Self-injection locked frequency conversion laser," Laser & Photonics Reviews **17**(5), 2200663 (2023).
- 203. J. Ling, Z. Gao, S. Xue, et al., "Electrically empowered microcomb laser," Nat. Commun. 15(1), 4192 (2024).
- 204. C. Op de Beeck, F. M. Mayor, S. Cuyvers, et al., "III/V-on-lithium niobate amplifiers and lasers," Optica 8(10), 1288 (2021)
- 205. Y. Maeda, H. Nishi, N.-P. Diamantopoulos, et al., "Micro-transfer-printed inp-based membrane photonic devices on thin-film lithium niobate platform," J. Lightwave Technol. 42(11), 4023–4030 (2024).
- 206. X. Zhang, X. Liu, L. Liu, et al., "Heterogeneous integration of III-V semiconductor lasers on thin-film lithium
- niobite platform by wafer bonding," Appl. Phys. Lett. **122**(8), 081103 (2023). 207. T. J. Morin, J. Peters, M. Li, *et al.*, "Coprocessed heterogeneous near-infrared lasers on thin-film lithium niobate," Opt. Lett. 49(5), 1197-1200 (2024).
- 208. M. Li, C. Xiang, J. Peters, et al., "Heterogeneously-integrated self-injection locked lasers on thin film lithium niobate," in Optical Fiber Communication Conference, (Optica Publishing Group, 2024), W1K. 3.
- 209. M. Li, C. Xiang, J. Guo, et al., "Heterogeneously-integrated electro-optical transmitter with thin film lithium niobate," CLEO 4240026 AA127 (2025).
- 210. B. J. Shastri, A. N. Tait, T. Ferreira de Lima, et al., "Photonics for artificial intelligence and neuromorphic computing," Nat. Photonics 15(2), 102-114 (2021).
- 211. H. Li, B. Casper, G. Balamurugan, et al., "A 112 Gb/s PAM4 silicon photonics transmitter with microring modulator and CMOS driver," J. Lightwave Technol. 38(1), 131-138 (2020).
- 212. X. Wu, D. Huang, T. Kim, et al., "Fully integrated dual-polarization silicon photonic transceiver with automated polarization control," in Optical Fiber Communication Conference, (Optica Publishing Group, 2023), Tu2E. 3.
- 213. X. Wu, "Fully integrated silicon photonic high-speed transmitter with ring-assisted Mach-Zehnder modulator," OFC W3A.3 (2024).
- 214. D. Huang, X. Wu, S. Yerkes, et al., "Feedback Tolerant Quantum Dot Lasers Integrated With 300 mm Silicon Photonics," J. Lightwave Technol. **43**(4), 1855–1860 (2025).
- 215. S. Liu, X. Wu, D. Jung, et al., "High-channel-count 20 GHz passively mode-locked quantum dot laser directly grown on Si with 41 Tbit/s transmission capacity," Optica 6(2), 128 (2019).
- 216. S. Pan, H. Zhang, Z. Liu, et al., "Multi-wavelength 128 Gbit s-1 λ-1 PAM4 optical transmission enabled by a 100 GHz quantum dot mode-locked optical frequency comb," J. Phys. D: Appl. Phys. 55(14), 144001 (2022).
- 217. J. Chen, B. Yang, J. Qin, et al., "Energy efficient and high bandwidth quantum dot comb laser based silicon microring transmitter for optical interconnects," IEEE J. Select. Topics Quantum Electron. 31(2: Pwr. and Effic. Scaling in), 1–10 (2025).
- 218. G. Liu, P. J. Poole, Z. Lu, et al., "InAs/InP quantum dot mode-locked laser with an aggregate 12.544 Tbit/s transmission capacity," Opt. Express 30(3), 3205-3214 (2022).
- 219. Y. Geng, Y. Xiao, Q. Bai, et al., "Wavelength-division multiplexing communications using integrated soliton microcomb laser source," Opt. Lett. 47(23), 6129-6132 (2022).
- 220. M. M. Waldrop, "The chips are down for Moore's law," Nature 530(7589), 144-147 (2016).

- 221. T. Fu, J. Zhang, R. Sun, et al., "Optical neural networks: progress and challenges," Light: Sci. Appl. 13(1), 263 (2024).
- 222. B. Bai, H. Shu, X. Wang, et al., "Towards silicon photonic neural networks for artificial intelligence," Sci. China Inf. Sci. 63(6), 160403 (2020).
- J. Liu, Q. Wu, X. Sui, et al., "Research progress in optical neural networks: theory, applications and developments," PhotoniX 2(1), 5 (2021).
- 224. S. R. Ahmed, R. Baghdadi, M. Bernadskiy, *et al.*, "Universal photonic artificial intelligence acceleration," Nature **640**(8058), 368–374 (2025).
- 225. P. L. McMahon, "The physics of optical computing," Nat. Rev. Phys. 5(12), 717-734 (2023).
- 226. Z. Xue, T. Zhou, Z. Xu, et al., "Fully forward mode training for optical neural networks," Nature 632(8024), 280–286 (2024).
- J. Hu, D. Mengu, D. C. Tzarouchis, et al., "Diffractive optical computing in free space," Nat. Commun. 15(1), 1525 (2024).
- 228. Y. Shen, N. C. Harris, S. Skirlo, *et al.*, "Deep learning with coherent nanophotonic circuits," Nat. Photonics **11**(7), 441–446 (2017).
- 229. S. Xu, J. Wang, H. Shu, *et al.*, "Optical coherent dot-product chip for sophisticated deep learning regression," Light: Sci. Appl. **10**(1), 221 (2021).
- 230. S. Bandyopadhyay, A. Sludds, S. Krastanov, et al., "Single-chip photonic deep neural network with forward-only training," Nat. Photonics 18(12), 1335–1343 (2024).
- B. Dong, F. Bruckerhoff-Pluckelmann, L. Meyer, et al., "Partial coherence enhances parallelized photonic computing," Nature 632(8023), 55–62 (2024).
- 232. T. Z. Zhihao Xu, M. Ma, C. Deng, et al., "Large-scale photonic chiplet Taichi empowers 160-TOPS/W artificial general intelligence," Science 384(6692), 202–209 (2024).
- 233. Z. Chen, A. Sludds, R. Davis, *et al.*, "Deep learning with coherent VCSEL neural networks," Nat. Photonics **17**(8), 723–730 (2023)
- 234. B. Ma and W. Zou, "Demonstration of a distributed feedback laser diode working as a graded-potential-signaling photonic neuron and its application to neuromorphic information processing," Sci. China Inf. Sci. 63(6), 160408
- 235. X. Guo, H. Zhou, S. Xiang, *et al.*, "Photonic reservoir computing system for pattern recognition based on an array of four distributed feedback lasers," ACS Photonics **11**(3), 1327–1334 (2024).
- 236. Z. Dai, X. Guo, S. Xiang, et al., "Photonic spiking reservoir computing system based on a DFB-SA laser for pattern recognition," ACS Photonics 12(2), 989–996 (2025).
- 237. X. Meng, G. Zhang, N. Shi, et al., "Compact optical convolution processing unit based on multimode interference," Nat. Commun. 14(1), 3000 (2023).
- 238. S. Hua, E. Divita, S. Yu, et al., "An integrated large-scale photonic accelerator with ultralow latency," Nature **640**(8058), 361–367 (2025).
- L. Chang, S. Liu, and J. E. Bowers, "Integrated optical frequency comb technologies," Nat. Photonics 16(2), 95–108 (2022).
- 240. X. Xu, M. Tan, B. Corcoran, *et al.*, "11 TOPS photonic convolutional accelerator for optical neural networks," Nature **589**(7840), 44–51 (2021).
- 241. Y. Wu, Q. Yang, B. Shen, *et al.*, "Multifunctional mixed analog/digital signal processor based on integrated photonics," Opto-Electronic Science **3**(8), 240012 (2024).
- 242. J. Feldmann, N. Youngblood, M. Karpov, *et al.*, "Parallel convolutional processing using an integrated photonic tensor core," Nature **589**(7840), 52–58 (2021).
- 243. B. Bai, Q. Yang, H. Shu, *et al.*, "Microcomb-based integrated photonic processing unit," Nat. Commun. **14**(1), 66 (2023).
- 244. H. Feng, T. Ge, X. Guo, *et al.*, "Integrated lithium niobate microwave photonic processing engine," Nature **627**(8002), 80–87 (2024).
- 245. Z. Lin, B. J. Shastri, S. Yu, et al., "120 GOPS Photonic tensor core in thin-film lithium niobate for inference and in situ training," Nat. Commun. 15(1), 9081 (2024).
- 246. Z. Zhou, "On-chip quantum dot lasers driven high-speed optical neural networks," CLEO SW3H.1 (2024).
- 247. Z. Zhou, W. He, Y. Xie, et al., "On-chip quantum dot lasers for photonic processing unit on silicon-based heterogeneous platform," in 2024 IEEE Photonics Conference (IPC), (2024), pp. 1–2.
- 248. S. Ulbrich, T. Menzel, A. Reschka, et al., "Defining and substantiating the terms scene, situation, and scenario for automated driving," in 2015 IEEE 18th international conference on intelligent transportation systems, (IEEE, 2015), 982–988.
- 249. E. Marti, M. A. De Miguel, F. Garcia, et al., "A review of sensor technologies for perception in automated driving," IEEE Intell. Transport. Syst. Mag. 11(4), 94–108 (2019).
- 250. Y. Li and J. Ibanez-Guzman, "Lidar for autonomous driving: The principles, challenges, and trends for automotive lidar and perception systems," IEEE Signal Process. Mag. 37(4), 50–61 (2020).
- 251. N. Li, C. P. Ho, J. Xue, et al., "A progress review on solid-state LiDAR and nanophotonics-based LiDAR sensors," Laser & Photonics Reviews 16(11), 2100511 (2022).

- 252. J. K. Doylend and S. Gupta, "An overview of silicon photonics for LIDAR," Silicon Photonics XV 11285, 17–115 (2020).
- 253. F. Falconi, S. Melo, F. Scotti, *et al.*, "A combined radar & lidar system based on integrated photonics in silicon-on-insulator," J. Lightwave Technol. **39**(1), 17–23 (2021).
- 254. C.-P. Hsu, B. Li, B. Solano-Rivas, *et al.*, "A review and perspective on optical phased array for automotive LiDAR," IEEE J. Select. Topics Quantum Electron. **27**(1), 1–16 (2021).
- 255. W. Xu, Q. Yuan, Y. Yang, *et al.*, "Progress and prospects for LiDAR-oriented optical phased arrays based on photonic integrated circuits," npj Nanophotonics **2**(1), 14 (2025).
- 256. L. Huang, C. Yang, L. Liang, et al., "Integrated light sources based on micro-ring resonators for chip-based LiDAR," Laser & Photonics Reviews 19(2), 2400343 (2025).
- 257. X. Sun, L. Zhang, Q. Zhang, et al., "Si photonics for practical LiDAR solutions," Applied Sciences 9(20), 4225
- 258. C. V. Poulton, M. J. Byrd, P. Russo, *et al.*, "Long-range LiDAR and free-space data communication with high-performance optical phased arrays," IEEE J. Select. Topics Quantum Electron. **25**(5), 1–8 (2019).
- 259. C. Rogers, A. Y. Piggott, D. J. Thomson, et al., "A universal 3D imaging sensor on a silicon photonics platform," Nature 590(7845), 256–261 (2021).
- 260. S. A. Miller, Y.-C. Chang, C. T. Phare, et al., "Large-scale optical phased array using a low-power multi-pass silicon photonic platform," Optica 7(1), 3 (2020).
- X. Zhang, K. Kwon, J. Henriksson, et al., "A large-scale microelectromechanical-systems-based silicon photonics LiDAR," Nature 603(7900), 253–258 (2022).
- 262. K. Van Acoleyen, W. Bogaerts, J. Jágerská, *et al.*, "Off-chip beam steering with a one-dimensional optical phased array on silicon-on-insulator," Opt. Lett. **34**(9), 1477–1479 (2009).
- 263. J. Sun, E. Timurdogan, A. Yaacobi, et al., "Large-scale nanophotonic phased array," Nature 493(7431), 195–199 (2013).
- 264. J. Sun, E. S. Hosseini, A. Yaacobi, *et al.*, "Two-dimensional apodized silicon photonic phased arrays," Opt. Lett. **39**(2), 367–370 (2014).
- 265. A. Martin, P. Verheyen, P. De Heyn, et al., "Photonic integrated circuit-based FMCW coherent LiDAR," J. Lightwave Technol. 36(19), 4640–4645 (2018).
- 266. R. Chen, H. Shu, B. Shen, et al., "Breaking the temporal and frequency congestion of LiDAR by parallel chaos," Nat. Photonics 17(4), 306–314 (2023).
- 267. J. Hulme, J. Doylend, M. Heck, et al., "Fully integrated hybrid silicon two dimensional beam scanner," Opt. Express 23(5), 5861–5874 (2015).
- 268. W. Xie, T. Komljenovic, J. Huang, et al., "Heterogeneous silicon photonics sensing for autonomous cars," Opt. Express 27(3), 3642–3663 (2019).
- 269. K. Sayyah, R. Sarkissian, P. Patterson, et al., "Fully integrated FMCW LiDAR optical engine on a single silicon chip," J. Lightwave Technol. 40(9), 2763–2772 (2022).
- 270. C. V. Poulton, M. J. Byrd, M. Raval, *et al.*, "Large-scale silicon nitride nanophotonic phased arrays at infrared and visible wavelengths," Opt. Lett. **42**(1), 21–24 (2017).
- 271. Q. Wang, S. Wang, L. Jia, et al., "Silicon nitride assisted 1 × 64 optical phased array based on a SOI platform," Opt. Express 29(7), 10509–10517 (2021).
- 272. W. Xu, Y. Guo, X. Li, *et al.*, "Fully integrated solid-state LiDAR transmitter on a multi-layer silicon-nitride-on-silicon photonic platform," J. Lightwave Technol. **41**(3), 832–840 (2023).
- 273. A. Lukashchuk, H. K. Yildirim, A. Bancora, et al., "Photonic-electronic integrated circuit-based coherent LiDAR engine," Nat. Commun. 15(1), 3134 (2024).
- 274. V. Snigirev, A. Riedhauser, G. Lihachev, et al., "Ultrafast tunable lasers using lithium niobate integrated photonics," Nature 615(7952), 411–417 (2023).
- 275. S. Xue, M. Li, R. Lopez-Rios, et al., "Pockels laser directly driving ultrafast optical metrology," Light: Sci. Appl. 14(1), 209 (2025).